# Long-term hazard assessment of explosive eruptions at Jan Mayen Island (Norway) and implications on air-traffic in the North Atlantic

Manuel Titos[1], Beatriz Martinez Montesinos[2], Sara Barsotti[1], Laura Sandri[2], Arnau Folch[3,4], Leonardo Mingari[3], Giovanni Macedonio[5], and Antonio Costa[2]

[1]Icelandic Meteorological Office (IMO), Iceland
[2]Istituto Nazionale di Geofisica e Vulcanologia, Sezione di Bologna, Italy
[3]Barcelona Supercomputing Center (BSC), Spain
[4]Geociencias Barcelona, Consejo Superior Investigaciones Cientificas, (CSIC), Spain
[5]Istituto Nazionale di Geofisica e Vulcanologia, Osservatorio Vesuviano, Italy

**Correspondence:** Manuel Titos (manuel@vedur.is)

**Abstract.** Volcanic eruptions are amongst the most jeopardizing natural events due to their potential impacts on life, assets, and environment. In particular, atmospheric dispersal of volcanic tephra and aerosols during the explosive eruptions poses a serious threat to life and has significant consequences for infrastructures and global aviation safety. The volcanic island of Jan Mayen, located in the North Atlantic under trans-continental air traffic routes, is considered the northernmost active volcanic area in the world, with at least ~~five~~ 5 eruptive periods recorded during the last 200 years. However, quantitative hazard assessments on the possible consequences for air traffic of a future ash-forming eruption at Jan Mayen are nonexistent. This study presents the first comprehensive long-term volcanic hazard assessment for Jan Mayen volcanic island in terms of ash dispersal and ~~airborne tephra~~ concentration at different flight levels. In order to delve in the characterization and modelling of that potential impact, a probabilistic approach based on merging a large number of numerical simulations is adopted, varying the volcano's ~~Eruptive~~ Eruption Source Parameters (ESPs) and meteorological scenario. Each ESP value is randomly sampled following a continuous Probability Density Function (PDF) ~~defined from~~ based on the Jan Mayen geological record. Over 20 years of ~~climatic~~ meteorological data are considered in order to explore the natural variability associated with ~~meteorological~~ weather conditions and used to run thousands of simulations of the ash dispersal model FALL3D on a 2 km-resolution grid. The simulated scenarios are combined to produce probability maps of airborne ash concentration, arrival time and persistence ~~at different flight levels~~ of unfavorable conditions at flight levels 50 and 250 (FL050 and FL250). The resulting maps can represent an aid to civil protection, decision makers and, moreover, aviation stakeholders in assessing and preventing the potential impact from a future ash-rich eruption at Jan Mayen.

## 1 Introduction

Along with earthquakes, tsunamis and weather extremes, explosive volcanic activity is amongst the most threatening natural hazards, with potential to contribute to global warming and environmental changes ~~(e.g. Ward, 2015)~~(Ward, 2015). The impacts of volcanic emissions can extend over large distances from the source, posing a threat to human health and jeopardizing air nav-

igation. Some recent examples of events leading to millionaire losses due to air traffic disruption include the eruptions in Eyjafjallajökull (Iceland, 2010), Grímsvötn (Iceland, 2011) and Puyehue-Cordón Caulle (Chile, 2011) ~~(Budd et al., 2011; Elissondo et al., 2016;~~ (Mazzocchi et al., 2010; Oxford-economics, 2010; Tesche et al., 2012; Karlsdóttir et al., 2012; Budd et al., 2011; Elissondo et al., 2016) . These events were a stark ~~remainder~~ reminder on the importance of volcanic hazard assessment and related quantification of impacts of future eruptions, both essential tools to advise governments, aviation stakeholders and the society in general, contributing, in this way, to their preparedness. In 2019, before the ~~covid-19 pandemics~~ COVID-19 pandemics aviation break, Icelandic airports received around 8M passengers (7M international and 0.7M domestic) on a total of 181k flights ~~()~~(Isavia, 2019) . In turn, polar air traffic routes had shown a marked increase over the last years, with a 15-fold increase between 2003 and 2015, and reaching more than 14k flights yearly since 2016 ~~()~~(NavCanada, 2017; Stewart-Green, 2016).

Although Jan Mayen (JM) volcano tephrochronology reveals at least 8 eruptive periods over the last 600 years, 5 of them concentrated in the last 200 years (Gjerløw et al., 2016), the potential impact on air traffic following a future ash-forming eruption has never been assessed. According to ~~(Gjerløw et al., 2016)~~Gjerløw et al. (2016), the most likely volcanism at ~~Jan Mayen~~ JM island is characterized by effusive Hawaiian to violent Strombolian eruptions and, to a lesser extent, by lava domes and Surtseyan eruptions. However, due to the possibility of magma interacting with sea water, snow or ice, the likelihood of moderately to highly explosive eruptions is considerable. Historical distal records of trachytic tephra found in Ireland (Hunt, 2004) and basaltic tephra found in older sedimentary records in the North-Atlantic (Lacasse and Garbe-Schönberg, 2001; Brendryen et al., 2010; Voelker and Haflidason, 2015) or in Greenland ice-cores (Abbott and Davies, 2012) show the potential for producing Plinian explosive eruptions, whose size and frequency are, however, highly uncertain.

This paper presents the first comprehensive long-term Probabilistic Volcanic Hazard Assessment (PVHA) for ~~Jan Mayen~~ JM volcanic island focused on the potential impact of airborne tephra concentration on arctic and north-Atlantic air routes. This is done by using the FALL3D model (Folch et al., 2009, 2020) to simulate the transport of ash clouds and its concentration at ~~two different~~ two relevant flight levels over a geographical area of approx 2000 km x 2000 km covering Iceland and the U.K.

In order to account for the natural variability in volcanic eruption intensity, vent position and wind field, ~~we follow~~ two main steps have been followed as suggested in ~~(Sandri et al., 2016)~~Sandri et al. (2016).

First, ~~by using field work~~ based on field data, we identify the possible eruptive ~~categories for Jan Mayen~~ classes for JM volcano and then we define a ~~probability distribution function~~ Probability Density Function (PDF) to describe the relative probability of the different ~~categories~~ classes to occur. For each ~~category~~class, we then define PDFs for each eruptive parameter (such as eruption duration or total erupted mass) in order to account for the natural variability of the eruption conditions. Then, by randomly sampling these PDFs, we generate a large dataset of ~~eruptive source parameters~~ ESP to be used ~~in input to the model~~ as model input. A novel strategy ~~has been developed~~ is proposed to treat and describe the styles of pulsating eruptions, characterized by a series of discrete short-lived events followed by occasional interruption of ~~the~~ tephra emission. Secondly, to fully explore the natural variability of the meteorological conditions, the numerical simulations have been randomly initialized within the period ~~01-01-1999 - 01-01-2020 (20~~ 1999-2020 (21 years). The meteorological data have been obtained from ERA5 reanalysis dataset ~~().~~ and FALL3D ~~has been run~~ used to generate thousands simulations per representative eruptive scenario. As a result, the following questions are answered:

- which is the probability that, in case of an eruption at JM, the ash cloud concentration will exceed the critical condition for safe flights within a domain extending down to the U.K. airspace after 3, 6, 12, 24 hours since the beginning of the eruption?
- in case of an eruption at JM, which is the probability that airports in Iceland and U.K. will be affected by the presence of ash?
- which is the probability to exceed a predefined hazardous temporal persistence of unsafe flight conditions?
- which flight level (FL) is likely to be predominantly affected by critical concentrations of volcanic ash?

The rest of the paper is organized as follows: ~~section~~Section 2 provides a historical overview of the Holocene volcanic activity of ~~Jan Mayen~~ JM volcano. Section 3 describes the most likely eruptive ~~categories~~ classes based on the five historical known eruptions of ~~Jan Mayen;~~ JM, fits them into a ~~Probability Density Function (PDF )~~ PDF for the total erupted volume~~and address~~ , addresses a novel strategy to treat and ~~describe~~ describes the styles of pulsating eruptions. Sections 4 and 5 present results and discussions~~.~~ , and finally, Section 6 concludes the study.

## 2 Jan Mayen Volcanism

~~Jan Mayen~~ JM is a Norwegian volcanic island located in the North-Atlantic Ocean at 71° N, 8° W around 600 km ~~north~~ North of Iceland, in the Norwegian Greenland Sea (Fig. 1). According to ~~(Kandilarov et al., 2012)~~Kandilarov et al. (2012); Larsen et al. (2021) , Jan Mayen microcontinent (JMMC, Fig. 2a) is a structural entity enclosing the Jan Mayen Ridge (JMR) and the surrounding area, including the Jan Mayen Basin (JMB), the Jan Mayen Basin South (JMBS), the Jan Mayen Trough (JMT), and the Southern Ridge Complex (SRC) (see Fig. 2b). To the north, JMMC is bordered by the Jan Mayen Fracture Zone (JMFZ) and the volcanic complex of Jan Mayen Island, while to the ~~south, east and west~~ South, East and West it borders by the NE coastal shelf of Iceland (NIS), the Norway Basin and the Kolbeinsey Ridge (KBR), respectively (Fig. 2a). Although the historic activity reports at least five eruptive periods over the last 200 years (since the discovering of the island at the beginning of the 17th century) (Gjerløw et al., 2016), its Holocene eruptive history is basically unknown. In this sense, the eruptive history of ~~Jan Mayen~~ JM comprises only a very few distal sediment cores as well as lava flows and tephra deposits from eruptions on the ice-free parts of the Beerenberg volcano. Distal records as trachytic tephra found in Ireland (Hunt, 2004) and basaltic tephra found in older sediment-records in the North-Atlantic (Lacasse and Garbe-Schönberg, 2001; Brendryen et al., 2010; Voelker and Haflidason, 2015) or in Greenland ice-cores (Abbott and Davies, 2012) have shown the potential for explosive ash-forming eruptions whose size, frequency, and potential impact are, however, uncertain. According to ~~(Imsland, 1978)~~Imsland (1978) , explosive hydromagmatic eruptions were common earlier in the history of ~~Jan Mayen~~JM. Nevertheless, as the island grew above sea level, such eruptions became less frequent and the volcanism essentially localized on two different regions: 1) the Beerenberg central volcano and its flank eruptions in northeastern part (called Nord-Jan) and, 2) the ~~Midt- and Sør-Jan~~ volcanic ridge extending ~~to the south-west. On the~~ from the middle to the southwestern part (called Midt-Jan and Sør-Jan respectively). On one hand, considering that the higher altitudes of the volcano are ice-covered and glacier tongues extend down to sea level

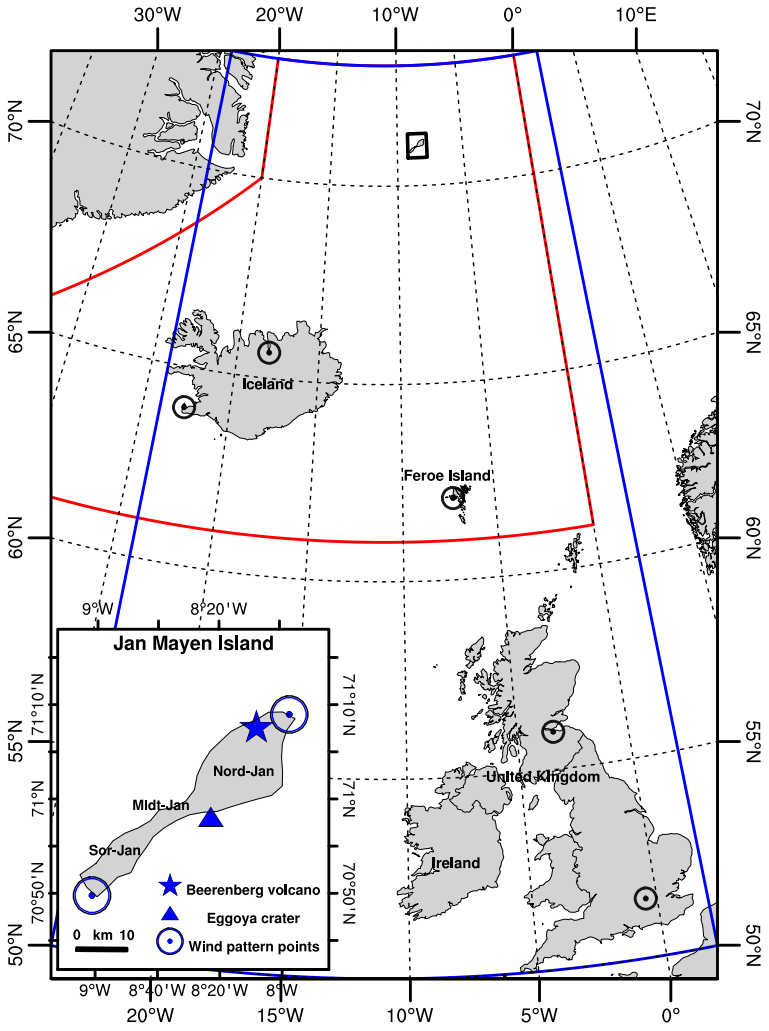


**Figure 1.** JM location and computational domain for the JM PVHA including Iceland, Ireland, and the United Kingdom (blue box). The red contour shows the FIR (Flight Information Region) for which Icelandic Meteorological Office is responsible (for visualization purposes only). The blue star and triangle in the zoomed map indicate the location of Beerenberg volcano and Eggoya crater (1732 Surtseyan eruption) respectively. The 2 blue circles show the 2 hypothetical vent locations in the wind profile analysis. Black circles correspond to Keflavik and Akureyri (Iceland), Vágar (Faroe Islands), Edinburgh (Scotland) and Heathrow (U.K., London) airports. Nord-Jan, Midt-Jan and Sør-Jan correspond to 3 areas in which JM is classically divided.

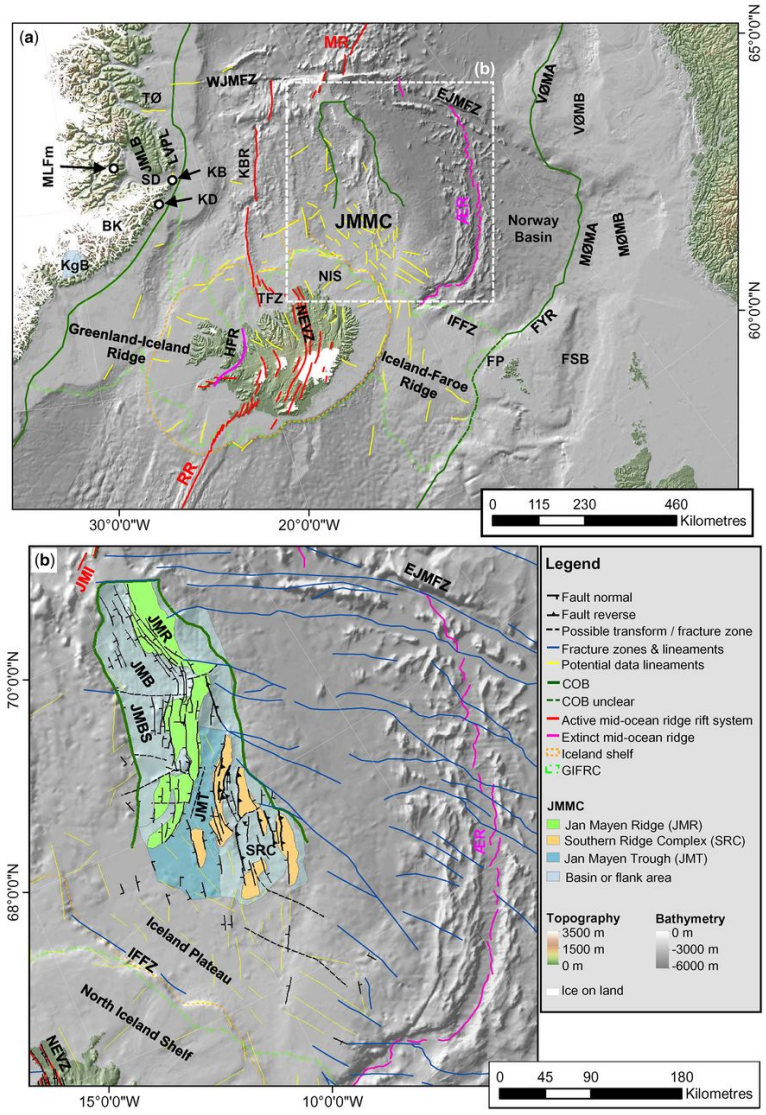


**Figure 2.** Overview map (a) of the study area with the location of structural elements identified on potential field data. Structural elements map (b) for the Jan Mayen microcontinent (JMMC): mapped faults, fractures zones and lineaments based on ~~(Peron-Pinvidic et al., 2012; Gernigon et al., 2015)~~Peron-Pinvidic et al. (2012); Gernigon et al. (2015). The background image is shaded bathymetry (IBCAO 3.0: (Jakobsson et al., 2012; Amante and Eakins, 2009)). Image retrieved from ~~(Blischke et al., 2017)~~ Blischke et al. (2017).

at several locations, the Holocene eruptions from the summit crater are difficult to map and no tephra layers have been positively linked to eruptions from the summit. Only a few land-based tephra records on the ice-free areas of Beerenberg have been mapped with some detail. Based on several sediment cores, ~~(Gjerløw et al., 2016)~~ Gjerløw et al. (2016) concludes that the Holocene volcanism on Beerenberg has been effusive or mildly explosive. As a result, the most common forms of recognized volcanic activity at Beerenberg are flank eruptions in the form of basaltic fissure and Strombolian to violent Strombolian eruptions. Eruption frequency is difficult to ~~be assessed~~ assess due to scarce reconstruction data. However, during historical times, the Beerenberg's eruption rate has been around 1 eruption every 60-70 years, with eruptive phases lasting in the range of days to months. During the most recent effusive eruption in 1970, the largest known one during the Holocene, the volume of lava flows was of at least 0.5 $km^3$ Dense Rock Equivalent (DRE) (Siggerud, 1972). On the other hand, volcanism on ~~Midt-~~Midt-Jan and Sør-Jan represents mostly effusive eruptions characterized by scoria cones, shallow marine to coastal phreatomagmatic eruptions, coulees and domes ~~()~~(Larsen and Guðmundsson, 2016; Gjerløw et al., 2015). The eruption frequency on this part of ~~Jan Mayen~~ JM is also difficult to assess due to erosion and superimposition of newer vents (possibly covering and removing older ones). However, considering visible evidence, the (under) estimated number of eruptions over the last 10k years is around 45, resulting in an eruption frequency of 1 eruption every 220 years. The duration of the eruptions from ~~Sør- and Midt-Jan~~ Midt and Sør-Jan is still unknown. The unrest episode recorded in 1732 (Eggoya, Midt-Jan), which led to the largest known explosive eruption, was a Surtseyan eruption that dispersed tephra over large parts of ~~Jan Mayen~~ JM and the surrounding seas. The volume of tephra ranges between 0.3-0.4 $km^3$ ~~.~~ (Gjerløw et al., 2015).

## 3 Methodology

### 3.1 Eruption scenarios

~~The possible~~ Despite the limitations of a complete geological record composed of both chronological and statistical data, the possible relative eruptive scenarios at JM are based on 5 historical and prehistorical known eruptions. According to the categorization proposed by Larsen and Guðmundsson (2016); Gjerløw et al. (2016), eruption scenarios can be characterised by small ($< 0.1$ $km^3$), moderate (0.1-0.5 $km^3$), large ($> 0.5$ $km^3$) DRE volumes or magnitudes (see Table 1) ~~, and Sub-Plinian~~ (Pyle, 2015), and sub-Plinian eruptions.

- Small eruptions are mostly effusive events characterised by small lava flows or small scoria cones, with erupted volumes ranging $10^7$-$10^8$ $m^3$ (total less than 0.1 $km^3$ DRE), corresponding to eruption magnitudes 1 to 2, hence VEI=~~2.~~ 2 (Newhall and Self, 1982). Based on historical occurrence, this scenario can last for about 35-40 hours.

- ~~Moderate~~ Medium eruptions include subaerial, sub-glacial and even ~~surtseyan~~ Surtseyan eruptions depending on within which environment they occur. Subaerial eruptions would be mainly located on Beerenberg volcano and they are expected to be effusive and/or Vulcanian to ~~Violent~~ violent Strombolian. When effusive, ~~moderate~~ medium eruptions are characterised by aa-lavas but also pahoehoe-flows. Surtseyan eruptions are expected to be located on ~~Jan Mayen~~ JM and

**Table 1.** Possible relative eruption scenarios on ~~Jan Mayen~~ JM Island. The categorization is based on the volume of tephra emitted in DRE. Data obtained from ~~, (Gjerløw et al., 2016)~~Larsen and Guðmundsson (2016); Gjerløw et al. (2016). According to the geological record (extending beyond the Holocene), subPlinian/Plinian events are highy unlikely (1%). Because of this, they are not included in this table.

| | Total Erupted Volume ($km^3$ (DRE)) | Eruption Magnitude | Eruption type (VEI) | Duration (hour/days) | Historical relat (Probal |
|---|---|---|---|---|---|
| Small | <0.1 | 1 to 2 | small lava flows or small ~~scoria cones~~ scoria cones. VEI=2 | 35-40 hours | 1 out 5 |
| Medium | 0.1-0.5 | 3 to 4 ~~Surtseyan eruption~~ | Effusive and/or ~~volcanian~~ Vulcanian to violent Strombolian Surtseyan. VEI=3 | 4-40 days possibly pulsating~~if Surtseyan~~ if Surtseyan | 2-3 out 5 ( |
| Large | >0.5 | 4 to 5 | Explosive and/or effusive VEI=4 | ~~1-4~~ 1-5 days | 1-2 out 5 ( |

the surrounding shallow part of the ocean. These eruptions consist of phreatomagmatic pulses, each of which, according to observations, can last for approximately 0.5-8 days, generate a volcanic plumes between 3 and 11 km ~~in high~~above sea level (a.s.l), and have a range of total erupted volume of $10^8$ –$10^{8.7}$ $m^3$ (~~total volume emitted would be between~~ 0.1~~and 0.5~~ –0.5 $km^3$ DRE), corresponding to eruption magnitudes 3 to 4, and VEI=3. The total duration of the eruption is not well constrained, as it can last between approximately 4 days and ~~one~~ 1 month. As a result, ~~ash fall~~ tephra-forming phases are expected, producing deposits more than one-meter thick within 5 km from the vent. The reference eruption for the Surtseyan type is the Eggoya 1732 AD eruption that produced at least 0.3-0.4 $km^3$ of tephra (0.16-0.21 $km^3$ DRE) ~~(Gjerløw et al., 2016)~~(Gjerløw et al., 2015, 2016).

– Large eruptions are expected to be initially subglacial and include moderate to sub-Plinian eruptions. During the opening phases, due to magma-ice interaction, the activity is explosive and characterised by plume heights reaching more than 10 km a.s.l and a range of total erupted volume of ~~$10^{8.7}$~$10^9$~~ $10^{8.7}$–$10^9$ $m^3$ (total volume emitted > 0.5 $km^3$ DRE), corresponding to eruption magnitudes of 4 to 5 and VEI=4. In this initial short-lasting explosive phase, a very small amount of tephra is expected to be ejected (approximately 5% of the total erupted mass). The reference eruption for this type is the 1970 event that produced at least 0.5 $km^3$ DRE (Siggerud, 1972). As the eruption proceeds it becomes more effusive lasting for 1-4 days.

– ~~Sub-Plinian~~ Very Large eruptions include sub-Plinian to Plinian eruptions characterised by column heights from 15 km to 25 km a.s.l and a range of total erupted volume of ~~$10^9$~$10^{9.7}$~~ $10^9$–$10^{9.7}$ $m^3$, hence eruption magnitudes of 5 to 6, corresponding to sub-Plinian type I or VEI ≥5. According to ~~(Gjerløw et al., 2016)~~Gjerløw et al. (2016), in the geological record (extending beyond Holocene) there is evidence of 10 tephra layers from subPlinian/Plinian events in 119k years. Because of this, we assign a subjective probability of 1% to this ~~category~~ class in case of eruption.

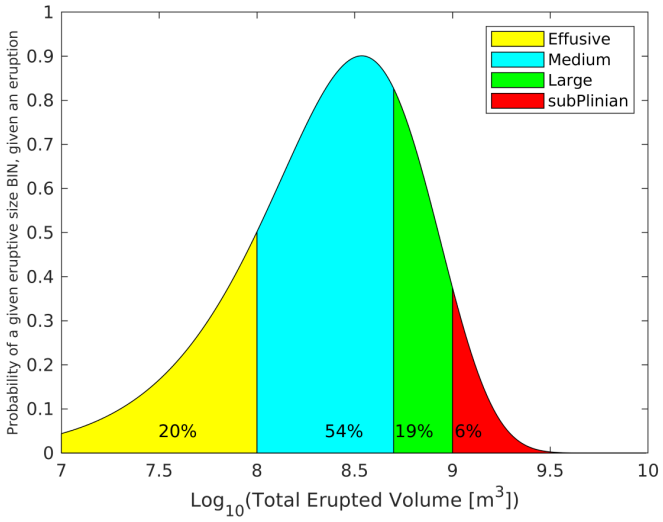


**Figure 3.** Weibull PDF describing the conditional probability of different eruptive magnitudes in case of an eruption at JM Island. The four colors cover the erupted volume ranges in the four "classical" eruption classes for JM, classically synthesized in 4 representative scenarios with a fixed mass, neglecting the variability in volume around these scenarios. The area under the different parts of the plot correspond to the probability of an Effusive, Medium, Large and subplinian class range eruption respectively, conditional to eruption occurrence. These values are in agreement with previous studies for JM (Larsen et al., 2017; Gjerløw et al., 2016).

### 3.2 Probabilistic hazard assessment approach

Until a few years ago, volcanic hazard assessment was largely based on the concept of "eruptive scenario", characterized by subjectively-defined eruption conditions. Hazard was then quantified under the strong assumption that the next eruption from a given volcano will be similar to the selected "representative eruptive scenario" (Macedonio et al., 2008; Barsotti et al., 2018)
145 . However, when assuming a representative eruptive scenario, one is implicitly neglecting the large uncertainties (both aleatory and epistemic) in the parameters that define the scenario also called "intra-size variability" ~~(e.g. Woodhouse et al., 2015; Harvey et al., 2018~~ . (Woodhouse et al., 2015; Harvey et al., 2018). More recent approaches try to circumvent the effects of natural variability by averaging hundreds of simulations where eruption parameters are sampled within a broad set of eruptive conditions in the so-called "eruption range scenarios" ~~(e.g. Bonadonna et al., 2005; Folch and Sulpizio, 2010; Harvey and Dacre, 2016; Prata et al., 2019)~~
150 (Bonadonna et al., 2005; Folch and Sulpizio, 2010; Prata et al., 2019). However, the use of a specific and limited range of eruption parameters continues introducing a large biased and uncertainties in the description of potential eruptive processes. For this reason, more recent approaches are based on the concept of a continuum of possible combinations of eruptive parameters, which translates into exploring a large set (many thousands) of simulations as proposed by ~~(Sandri et al., 2016; Sulpizio et al., 2012) . The natural approach to do it is by defining probability distributions within plausible ranges. As a consequence, eruption~~
155 Sulpizio et al. (2012); Sandri et al. (2016). Eruption parameters (e.g, total erupted mass, duration of the fallout phase, mass

eruption rate, total grain size distribution, etc.) are defined and randomly sampled from specific probability distributions (Sandri et al., 2016). The processes for sampling and weighting possible statistical combinations of values for the volcanological parameters corresponds to their probability of occurrence: this allows giving more/less weight to more/less likely combinations. ~~Weibull PDF describing the conditional probability of different eruptive magnitudes in case of an eruption for Jan Mayen Island. The four colors cover the erupted volume ranges in the four "classical" eruption categories for Jan Mayen, usually synthesized in 4 representative scenarios with a fixed mass, neglecting the variability in volume around these scenarios. The area under the different parts of the plot correspond to the probability of an Effusive, Medium, High and Subplinian category range eruption respectively, conditional to eruption occurrence. These values are in agreement with previous studies for Jan Mayen (Larsen et al., 2017; Gjerløw et al., 2016).~~ In order to explore the intra-size variability, we proceed as in ~~(Sandri et al., 2016)~~ Sandri et al. (2016):

1. A very broad range of possible eruptive ~~categories~~scenarios, characterized by the total erupted volume, is selected as explained in Section 3.1.

2. The total erupted volume is used to define the total erupted mass, the eruption magnitude, and the VEI.

3. The eruptive ~~category~~ range is split into eruption classes linked to representative members (see ~~section~~ Section 3.1), each characterized by an approximate conditional probability in the geological and historical record (see Table 1).

4. Over the total range of possible erupted volumes (approximately $10^7 - 10^{10}$ m$^3$), up to 6 different truncated Probability Density Functions (PDF) are tested to describe the conditional probability of these 4 mutually exclusive ~~categories~~classes: Normal, Exponential, LogLogistic, LogNormal, Gamma and Weibull. The best model is selected according to the Akaike~~Information Criteria~~'s Information Criterion (AIC) (Bozdogan, 1987; Akaike, 1998), where the relative goodness of fit of such PDFs (i.e., the likelihood of the catalog's frequencies of the different eruptive classes, under different PDFs) is compared, penalized by the number of parameters. The PDF with the lowest AIC is considered the best among all specified ones. Indeed, the assumption of a common PDF for the total erupted volume across the different eruption classes allows a smooth and coherent linking among them (Sandri et al., 2016). For JM, the Weibull PDF ~~(see Figure 3)~~ better fitted the expected frequencies on the sub-ranges for the 4 different eruption classes. This PDF is used to assign a conditional probability of occurrence to each simulation as a function of the associated total erupted volume (see Figure 3).

5. Considering the behavior of similar scenarios including wet plumes, for Medium and Large classes we account for ~~particle aggregates assuming different aggregate bin. They are~~ ash aggregation assuming two different aggregate types characterised by densities in the range of 250 and 350 kg/m$^3$ and diameters between 100 and 250 $\mu$m.

### 3.3 Pulsating eruptions: Modelling and strategy

A novel strategy is proposed to describe the styles and model dispersal from pulsating eruptions (Surtseyan eruptions, belonging to Medium class in Table 1), characterized by a series of discrete short-lived events followed by occasional interruption of the

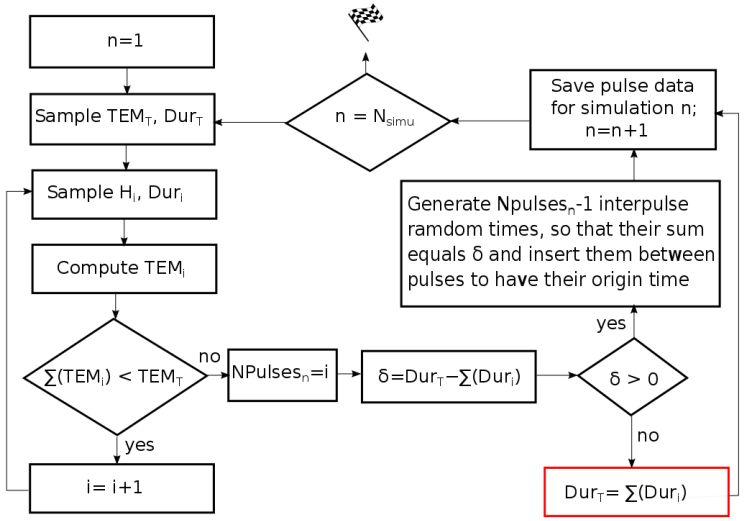


**Figure 4.** Proposed strategy to treat and describe the styles of pulsating eruptions, characterized by a series of discrete short-lived events followed by occasional interruption of the tephra emission.

emission of tephra. The strategy has been developed considering the ranges of all the ESP described in ~~section~~ Section 3.1. For each pulsating scenario, the ESP associated with column shape, total grain size distribution, and sphericity of tephra particles are also sampled from given PDFs. However, the difference is that column heights are not derived from the mass eruption rate but using the following approach (see Figure 4): ~~Proposed strategy to treat and describe the styles of pulsating eruptions, characterized by a series of discrete short-lived events followed by occasional interruption of the tephra emission.~~

1. Sampling randomly both the total erupted mass ($\text{TEM}_T$) and total duration of the eruption ($\text{Dur}_T$) considering values reflected in Section 3.1.

2. If the sum of masses erupted by all pulses does not equal or exceed the total erupted mass previously sampled, loop to:

   - Create the $i-th$ pulse sampling randomly column height ($\text{H}_i$) and duration ($\text{Dur}_i$). The duration is sampled from a normal distribution consistent with the data reflected in Table 1. The column height is sampled from a triangular distribution with lower limit 3 km, peak at 6 km, and upper limit 11 km a.s.l.
   - Compute the total erupted mass for such pulse ($\text{TEM}_i$) using the ~~(Mastin et al., 2009)~~ Mastin et al. (2009) relationship.
   - Compute ($\sum_{i=1}^{n}(\text{TEM}_i)$), being $n$ the number of pulses generated so far:
     - If ($\sum_{i=1}^{n}(\text{TEM}_i)$) > 0.97*$\text{TEM}_T$ and ($\sum_{i=1}^{n}(\text{TEM}_i)$) < $\text{TEM}_T$), modify $\text{TEM}_i$ to obtain $\sum_{i=1}^{n}(\text{TEM}_i) = \text{TEM}_T$, thereby avoiding small pulses. Compute the new column height ($\text{H}_i$) using ~~(Mastin et al., 2009)~~Mastin et al. (2009) .

– Else, if total erupted mass obtained ($\sum_{i=1}^{n}(\mathrm{TEM}_i)$) < $\mathrm{TEM}_T$, save the pulse. Otherwise, discard the pulse.

3. Compute the duration of the eruption as the sum of the duration of all the pulses ($\sum_{i=1}^{n}(Dur_i)$). If the $\sum_{i=1}^{n}(Dur_i) < Dur_T$, generate n-1 inter-pulses at random time ($Res_i$) so that their sum equals $\delta$ ($\delta$=$Dur_T - \sum_{i=1}^{n}(Dur_i)$) and insert them between pulses. Otherwise, if $\sum_{i=1}^{n}(Dur_i) > \mathrm{Dur}_T$, update $\mathrm{Dur}_T = \sum_{i=1}^{n}(Dur_i)$. This case actually supposes a continuous eruption where each pulse occurs without a rest period.

~~Computational domain for the JM PVHA including Iceland, Ireland, and the UK (blue box). The red contour shows the FIR (Flight Information Region) for which Icelandic Meteorological Office is responsible (for visualization purposes only). The blue star and triangle in the zoomed map indicate the location of Beerenberg volcano and Eggoya crater (1732 surtseyan eruption) respectively. The 2 blue circles show the 2 hypothetical vent locations in the wind profile analysis.~~

### 3.4 Vent location sensitivity

Given the scales of JM Island and the considered domain, the effects of the uncertain vent location on the resulting long-range hazard assessment can be expected to be negligible. In order to check this assumption we inspected how ERA5 wind profiles vary along the island by focusing on 2 vent locations at the NE (71.15º N, 7.95º W) and SW (70.82º N, 9.02º W) edges of the island, approximately 55 km apart (blue circles in Figure 1 inset). At these locations we inspected:

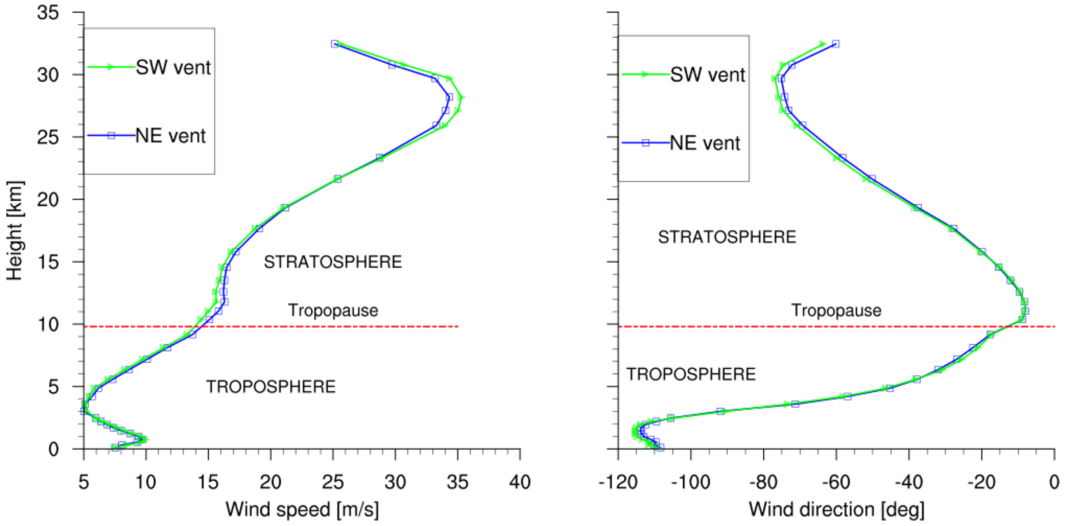


**Figure 5.** Monthly averaged ERA5 wind profiles (speed and direction) at 2 different locations (NE and SW) of ~~Jan Mayen~~ JM Island.

– Local wind profiles: Figure 5 shows vertical profiles of wind speed and direction averaged for the whole month of December, 2019. As observed, there are little differences in patterns between the two locations.

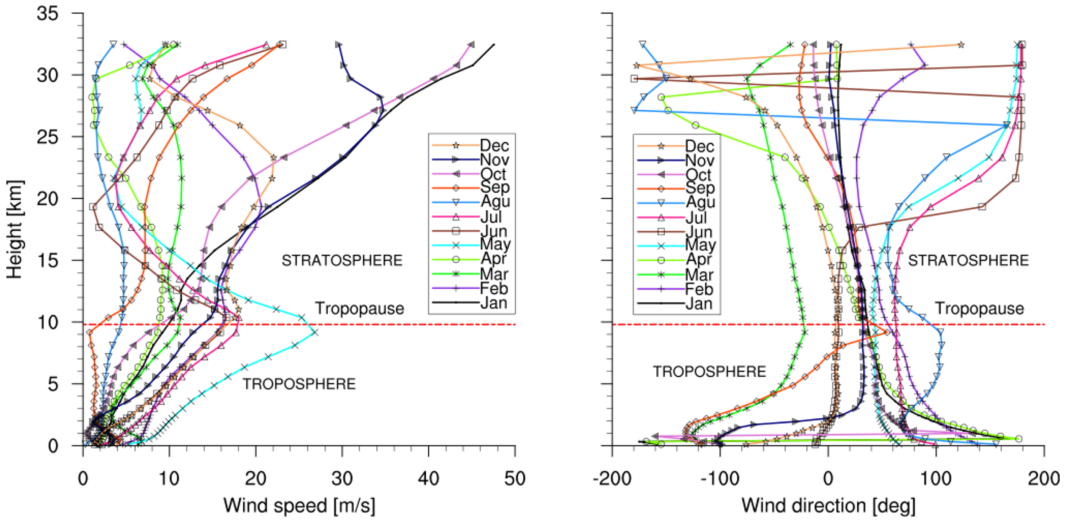


North-East vent

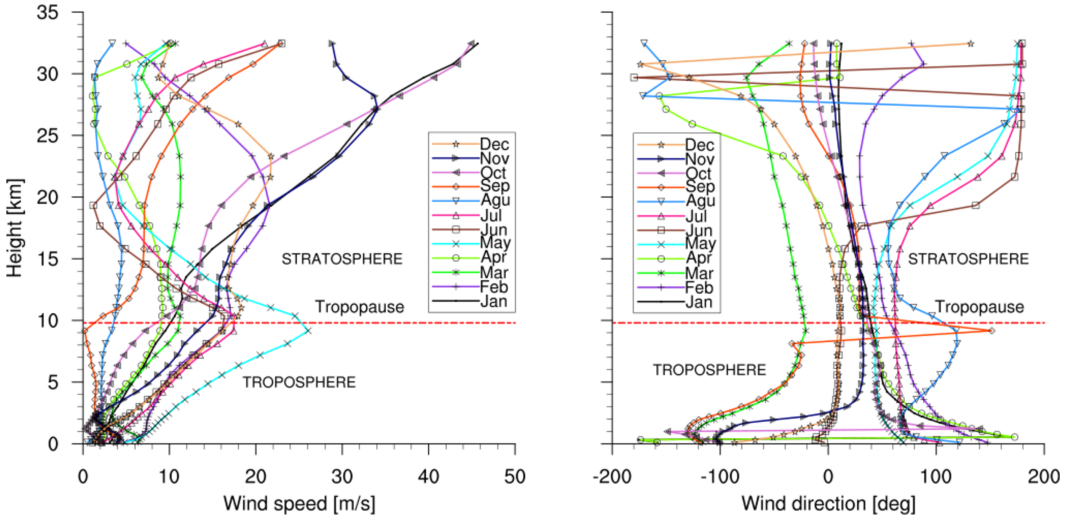


South-West vent

**Figure 6.** Monthly comparison of the wind pattern computed in 2 different locations (NE and SW) for a whole year, 2018. Top: Wind patterns corresponding to NE vent. Bottom: Wind patterns corresponding to SW vent. Results were obtained by averaging one year of ERA5 data.

– Annual wind profiles: Figure 6 shows the wind profiles averaged monthly for the year 2018. Once again, there are no differences between the two locations.

Considering the current limitation of both grid resolution and meteorological data resolution, the location of potential JM vents does not influence the ash dispersal pattern. As a result, we will not consider the uncertainty on the vent location and assume a fixed vent ~~at~~ in the middle of the island.

## 4 Results: Hazard maps and uncertainty quantification

### 4.1 ~~Hazard maps and uncertainty quantification~~

Hazard ~~maps~~ and probability maps (Elefante et al., 2010) are powerful tools to ~~provide information~~ inform on spatial and temporal potential impact of specific volcanic phenomena. Commonly, they consist of exceedance probability curves, referred to as hazard curves (Hill et al., 2013). These hazard curves quantify, in a grid point of the target domain and within a specific time window (exposure time) (Budnitz et al., 1997), the exceedance probability of an intensity measure threshold for a specific phenomenon (e.g., tephra load at ground level or airborne tephra concentration~~at two different flight levels~~).

~~In that regard, our~~ Our objective is to show the usefulness of ~~HPC-PVHA (~~probabilistic volcanic hazard assessment in the framework of High Performance Computing ~~)~~ evaluating the impact of low-probability but high-consequence events on air traffic (between Iceland and ~~UK~~U.K., see Figure 1) from a potential eruption at ~~Jan Mayen~~ JM Island, while quantifying how the ESP and wind patterns (velocity and direction) influence hazard and probability maps of ash dispersal and airborne tephra concentration.

~~In this study we try to answer the following questions:~~

- ~~which is the probability that, in case of an eruption in Jan Mayen, the ash cloud concentration will exceed the critical condition for safe flights within a domain extending down to the UK airspace after 3, 6, 12, 24 hours since the beginning of the eruption?~~
- ~~in case of an eruption in Jan Mayen, which is the probability that airports in Iceland and UK will be affected by the presence of ash?~~
- ~~which is the probability to exceed apredefined hazardous temporal persistence of unsafe flight conditions?~~
- ~~which flight level is likely to be predominantly affected by critical concentrations of volcanic ash ?~~

~~To this end, considering~~ Although our method allows analyzing any desired FL, in this work, only FL050 and FL250 (approx. 1.5 and 7.5 km a.s.l) will be analyzed. Such FLs were motivated considering standard cruise and maximum risk actions altitudes like takeoff or landing. Finally, three selected ash concentration thresholds (0.2, 2, and 4 mg/m$^3$) were selected based on the impacts of volcanic ash on jet engines summarized in Figure 7 and the considerations included in the Volcanic Ash Contingency Plan published by the International Civil Aviation Organization (ICAO, 2021). As a result, we analyze the results using isolines at ~~different flight levels for~~ FL050 and FL250 for these three selected ash concentration thresholds ~~(0.2, 2, and 4 mg/m$^3$),~~ through three different types of probabilistic maps:

- **Arrival time maps**: expected time required for the ash concentration to exceed ~~a given threshold (0.2,~~ 2 ~~, and 4~~ mg/m$^3$ ~~) at different flight levels~~ at FL050 with an exceedance probability of 5%, between 0 and 48 hours since the beginning of the eruption.

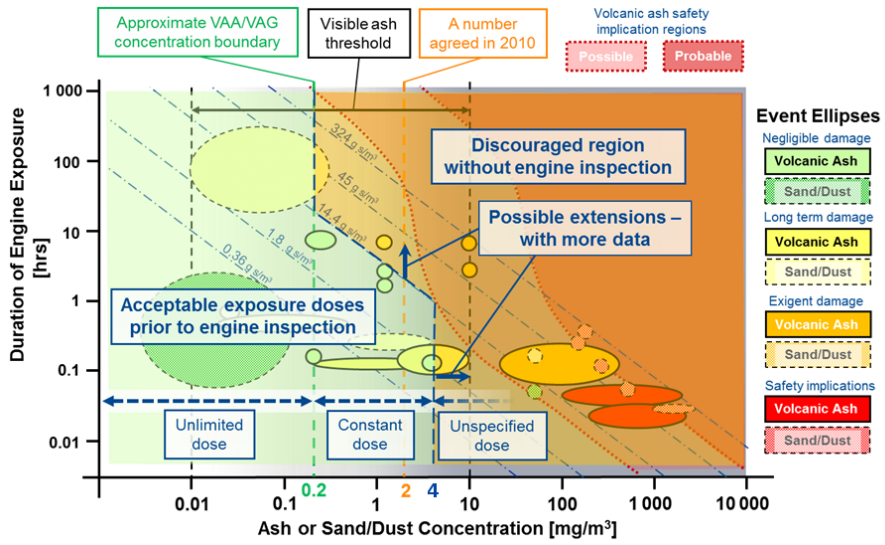


**Figure 7.** Overview of volcanic ash or sand/dust impacts on Jet Engines~~as provided by~~. Modified from Rolls-Royce review of aircrafts encountering airborne particle clouds ~~(Ellis et al., 2021; Rory, 2010)~~(Ellis et al., 2021; Clarkson et al., 2016).

– **Exceedance probability maps**: reporting the probability of reaching ash concentration above a given threshold (0.2, 2, and 4 mg/m$^3$) at ~~different flight levels and anytime during~~ FL050 and FL250 at some time from the onset of the eruption up to 48 hours after its end.

– **Persistence maps**: showing the fraction of hours (since the beginning of the eruption) during which the ash concentration exceeds a given threshold (0.2, 2 and 4 mg/m$^3$) with a probability larger than 5%~~probability~~.

Figure 8 depicts the arrival time maps for ~~large and medium~~ Large and Medium eruptions respectively. The % value in exceedance probability has been subjectively selected. However we highlight that our method allows a potential end user to explore any value of exceedance probability: here, ~~for the sake of brevity,~~ we only show the 5% maps as an example. ~~Arrival time required for the ash concentration (5000 feet or 1,5 km) to exceed a threshold of 2 mg/m$^3$ with an exceedance probability of 5% between 0 and 48 hours after eruption. Black circles correspond to the airports previously cited.~~ Figures 9 and ~~?? (D1 and ?? in the appendix)~~ D1 in the Appendix D show the probability of reaching or exceeding ash concentration above 0.2 mg/m$^3$, 2 mg/m$^3$, and 4 mg/m$^3$ at ~~different flight levels and anytime during~~ FL050 and FL250 at some time from the onset of the eruption up to 48 hours after its end for Large and Medium eruptive classes respectively.

~~Exceedance probability (Medium): probability of reaching or exceeding ash concentration above 0.2 mg/m$^3$ (left), 2 mg/m$^3$ (center) and 4 mg/m$^3$ (right) at 5000 feet at some time during the eruption up to 48 hours after its end.~~ ~~Knowing the extent and concentration of volcanic ash clouds requires temporal reasoning of the 3D domain given by thousands~~ Thousands of erup-

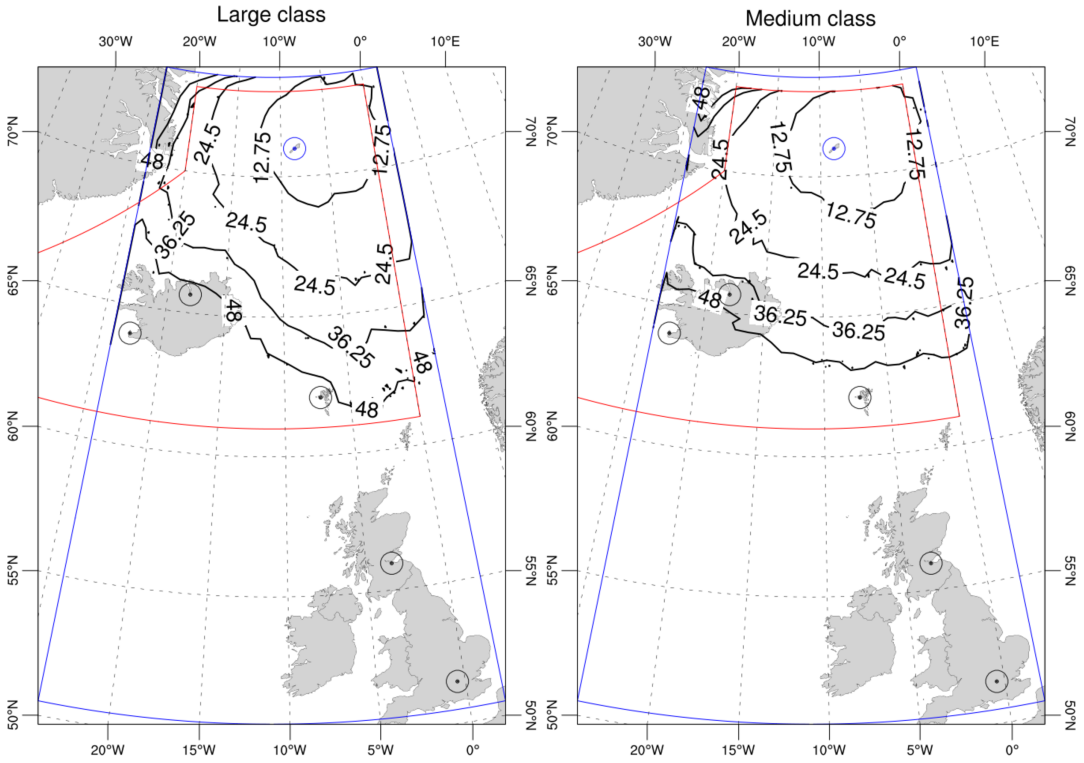


**Figure 8.** The Isolines show the arrival time in hours required for the ash concentration (at FL050) to exceed a threshold of 2 mg/m$^3$ with an exceedance probability of 5% between 0 and 48 hours after eruption. Black circles correspond to Keflavik and Akureyri (Iceland), Vágar (Faroe Islands), Edinburgh (Scotland) and Heathrow (U.K., London) airports.

tive scenarios ~~. In this regard, estimating knowledge uncertainty is essential to tackle the robustness of the results. Predictions made without~~ have been simulated to reproduce and capture, in a probabilistic way, the variability of a phenomena which can vary strongly in space and time. However, a proper uncertainty quantification (UQ) ~~do not quantify how constrained~~ is needed to quantify how reliable the prediction is~~, whereas ensembles members gives such an idea. It~~ . Such UQ can provide useful knowledge about the diversity of the dominant winds, the range in the airborne tephra concentration and its extent depending on the type of eruption, the ESP related to the eruption size, and the feature of pulsating events for Medium size eruptions. As a consequence, the threat evaluation and the spatio-temporal analysis presented here could bring forth a more robust comprehensive hazard assessment.

~~(Kristiansen et al., 2012) have~~ Kristiansen et al. (2012) concluded that the main source of epistemic/aleatory uncertainty in ash dispersal forecasts comes from the quantification of the eruption source term (eruption column height and emission rate). Here, we address the quantification of uncertainty over the airborne tephra concentration and its extent. To do that, we assess the 95% confidence interval (i.e., range between the 97.5 and 2.5 percentiles) in the probability distributions describing the hazard curves for the concentration of tephra for each point in the domain. These probability distributions are deeply related

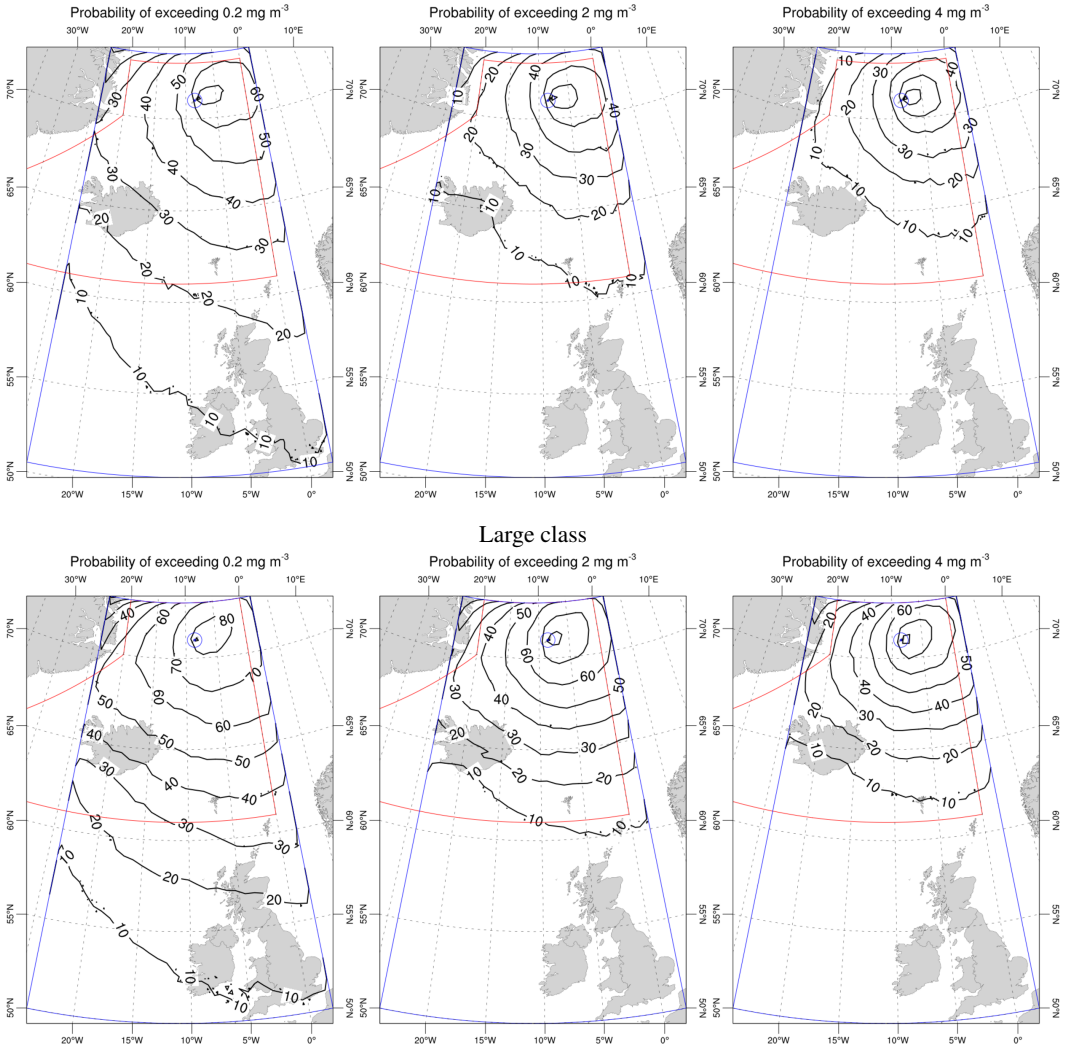


**Figure 9.** Exceedance probability ~~(Large)~~maps at FL050: the isolines show the probability of reaching ash concentration above 0.2 mg/m$^3$ (left), 2 mg/m$^3$ (center) and 4 mg/m$^3$ (right) at ~~5000 feet (or 1.5 km)~~ FL050 at some time ~~during~~ from the onset of the eruption up to 48 hours after its end. The three upper plots apply to the Large class and the three at the bottom to the Medium one.

to the number of simulations or scenarios used that model such concentrations, ~~so~~ a detailed analysis of how the number of simulations affects the sensitivity of this uncertainty can be found in the ~~appendix~~Appendix A.

290

~~Figures ?? and 10 , show~~ Figure 10 shows different maps, at different levels of confidence, produced by cutting the point-wise hazard curves at different percentiles. They correspond to a 4D analysis where concentrations are the highest at any time from the onset of the eruption up to 48 hours after its end.

~~Concentration hazard map (Large): relative uncertainties related with airborne ash cloud concentrations above 0.2 mg/m$^3$, 2~~

295 ~~mg/m$^3$ and 4 mg/m$^3$ and extent at 5000 feet (or 1.5 km). Each map corresponds to a different level of confidence, produced by cutting the hazard curves at different percentiles.~~

Figure 11 shows, from top-left to bottom-right, the probability of reaching or exceeding ash concentration above 2 mg/m$^3$ at ~~5000 feet elevation~~ FL050 for more than 1, 3, 6, 12, 18 and 24 hours, respectively, from the onset of a ~~large~~ Large eruption up to 48 hours after its end. Figure 12 shows the same but for the ~~medium-size-eruption~~ Medium-size-eruption and, in the

300 appendix, Figures D2 and D3 display the same information as Figures 11 and 12 but for ~~25000 feet~~FL250.

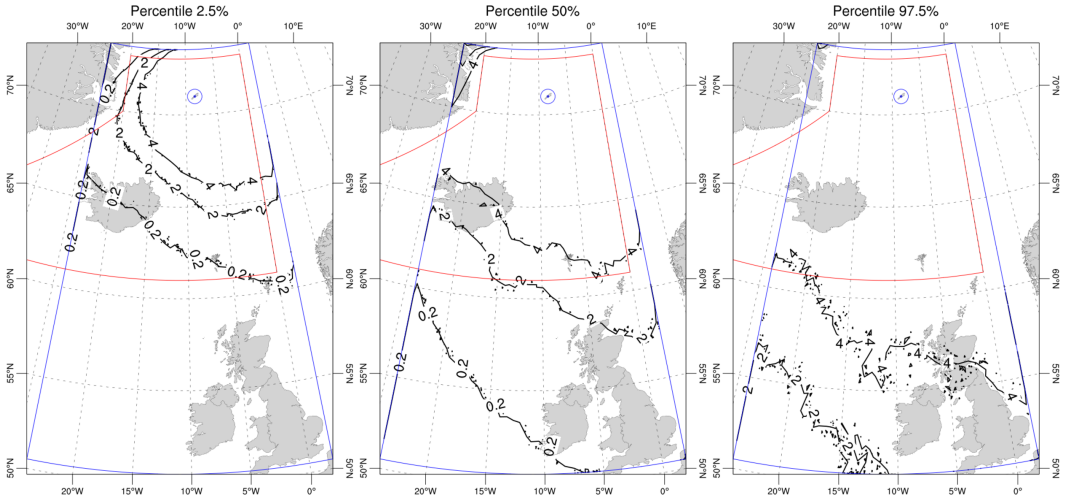


Large class

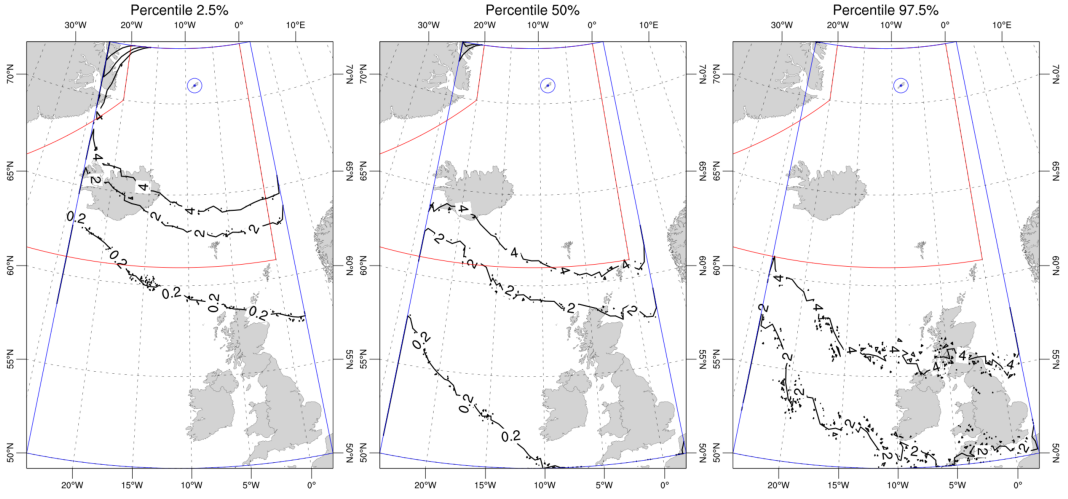


Medium class

**Figure 10.** Concentration extent hazard map ~~(Medium)~~at FL050: relative ~~epistemic~~ uncertainties related with airborne ash cloud concentrations above 0.2 mg/m$^3$, 2 mg/m$^3$ and 4 mg/m$^3$ and extent~~at 5000 feet (or 1.5 km)~~. Each map corresponds to a different level of confidence, produced by cutting the point-wise hazard curves at different percentiles.

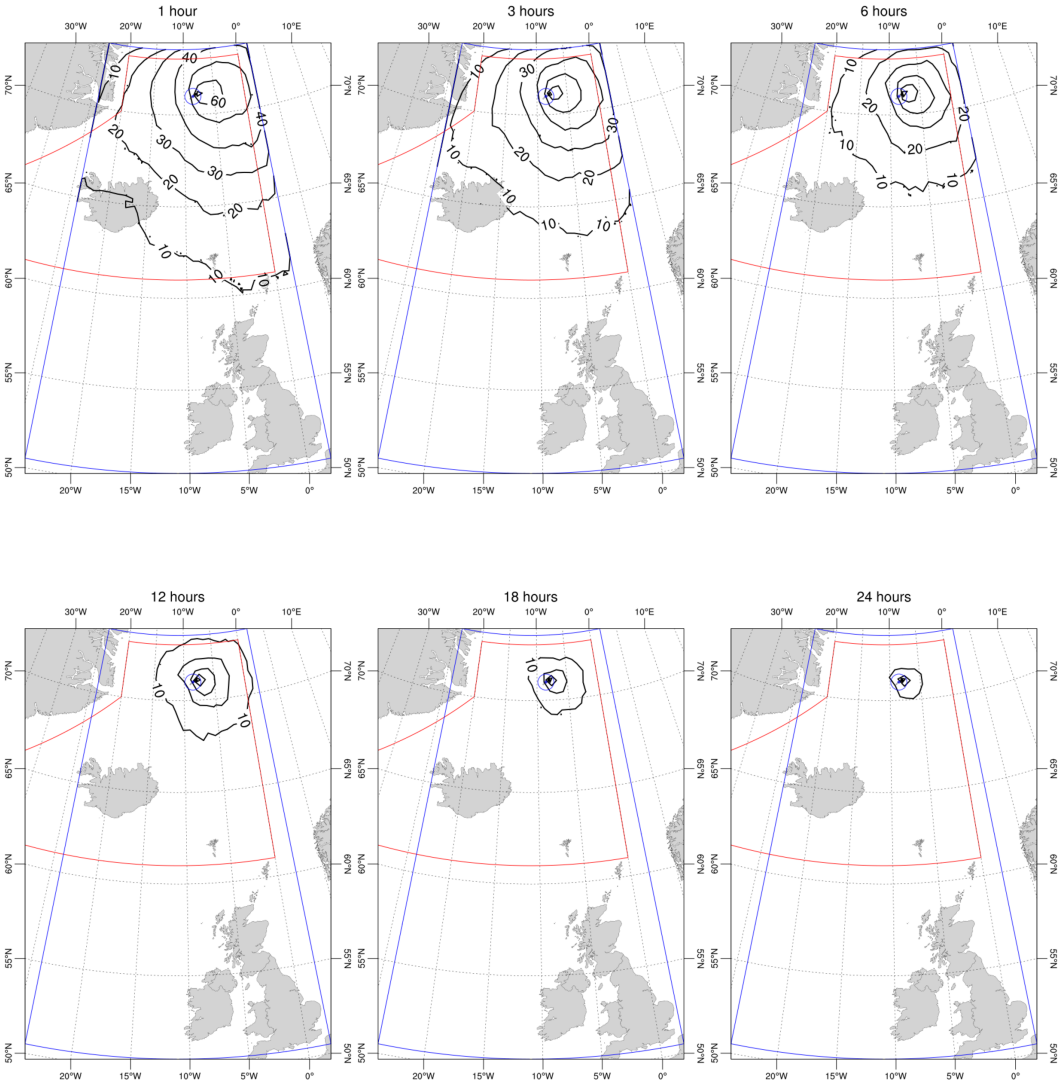


**Figure 11.** ~~Exceedance probability~~ Persistence maps at FL050 (Large class): the isolines show probability of reaching or exceeding ash concentration above 2 mg/m$^3$ at ~~5000 feet~~ FL050 1 hour, 3 hours, 6 hours, 12 hours, 18 hours, 24 hours during the eruption up to 48 hours after its end.

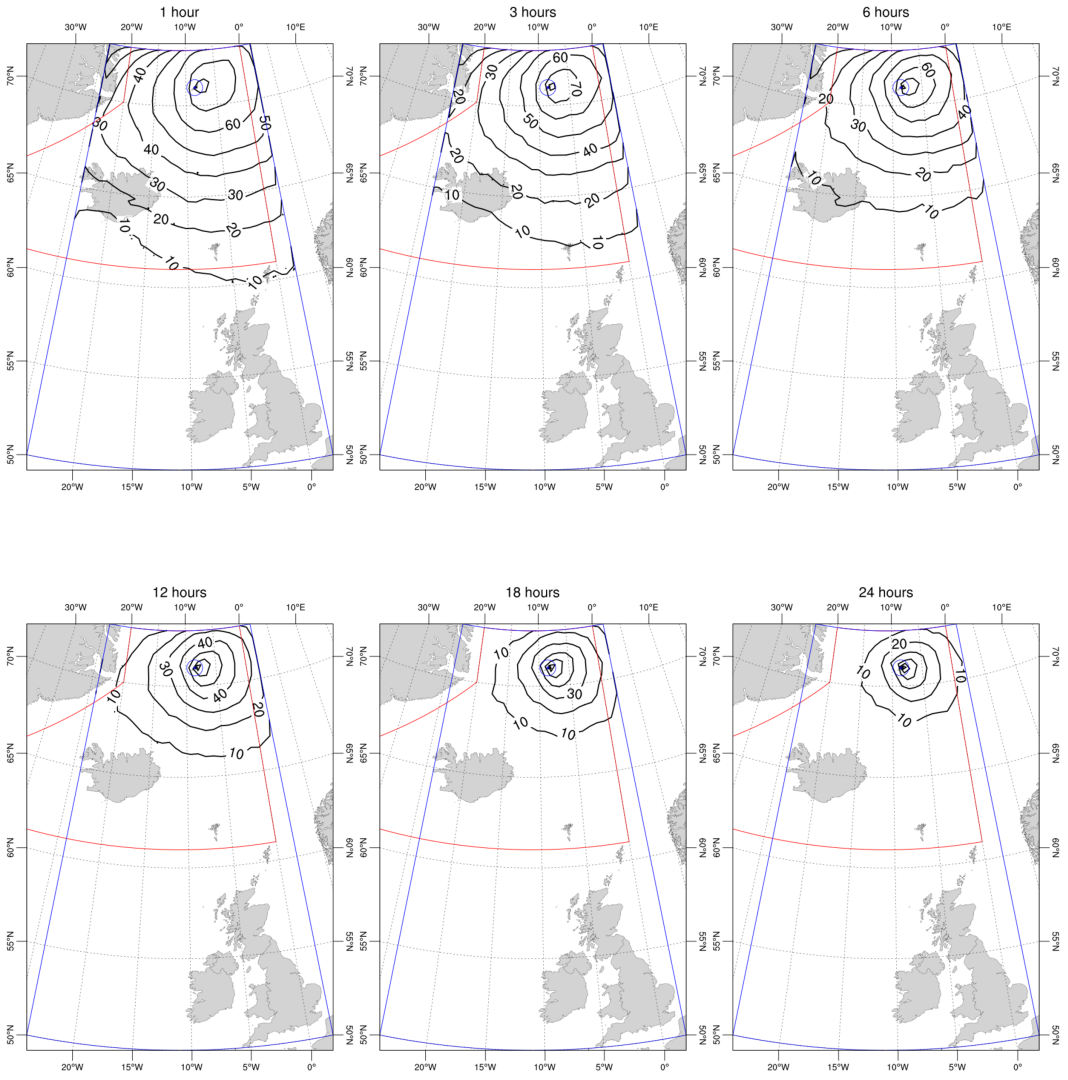


**Figure 12.** ~~Exceedance probability~~ Persistence maps at FL050 (Medium class): the isolines show probability of reaching or exceeding ash concentration above 2 mg/m$^3$ at ~~5000 feet~~ FL050 1 hour, 3 hours, 6 hours, 12 hours, 18 hours, 24 hours during the eruption up to 48 hours after its end.

**Table 2.** Airport locations, azimuth and distance to JM. Locations are expresed in Lat/Lon coordinates. Azimuth and distance correspond to azimut in degress and distance between JM Island and the different airports.

| | Location (Lat/Lon) | Azimuth (°) | Distance (km) |
|---|---|---|---|
| Akureyri (Iceland) | 65.658 N, 18.073 W | 218.25 | 712 |
| Keflavik (Iceland) | 63.986 N, 22.627 W | 224.50 | 981 |
| Vágar (Faroe Island) | 62.063 N, 7.277 W | 176.51 | 994 |
| Edinburgh (Scotland) | 55.948 N, 3.363 W | 169.11 | 1690 |
| Heathrow (England) | 51.472 N, 0.454 W | 165.25 | 2208 |

## 5 Discussion

~~In this section, we will discuss the results obtained for each type of analysis proposed in section ??~~Results have been carried out considering the intrinsic limitations of the methodology (partially due to the scarcity of data related with complete geological record composed of both chronological and statistical data). This fact is important, as future advances in the geological cataloge could have implications on future work assessing volcanic hazards and mitigating measures on JM. ~~Exceedance probabilities vs arrival times required for the ash concentration (5000 feet) to exceed a threshold of 2 mg/m$^3$ at different airports for medium and large eruptions since the beginning of the eruption.~~

### 5.1 Arrival time maps

~~Figure 8 depicts the expected time required for the ash concentration to exceed a threshold of 2 mg/m$^3$ with an exceedance probability of 5% between 0 and 48 hours after beginning of the eruption, for large and medium eruptions respectively. Among the most important conclusions, we can highlight that~~ As shown in Figure 8, an ash-rich eruption originating from ~~Jan Mayen~~ JM volcano has potential to affect the air traffic over Iceland ~~(~~after 36 hours ~~)~~ and, to some extent, the Faroe Island ~~,~~ or archipelago after 48 hours since the beginning of the eruption, with an exceedance probability of 5%.

Figure 13 shows the evolution of the probability over time of ~~having exceeded ash concentration of~~ ash concentration exceeding 2 mg/m$^3$ at ~~5000 feet~~ FL050 and at international airports of Keflavik and Akureyri (Iceland), Vágar (Faroe Islands) and ~~Luton and Heathrow (UK~~Heathrow (U.K., London) ~~since the beginning of the eruption. We can observe that the probability of exceeding the threshold~~ (see Table 2 for distance references). The probability at any airport is ~~almost zero~~ neglectable during the first hours (~~ten hours for the medium size~~ approx. 10 and 15 hours for ~~the large case, approximately) and~~ Medium and Large classes respectively) and then increases until stabilizing after several days (~~3 days for the large size and 10 days for the medium size, approximately). We can also see that, for~~ approx. 7 and 5 days for Medium and Large classes respectively). For both eruption classes, ~~although~~ Vágar airport ~~is further from the volcano, it~~ has a higher probability of exceeding ~~the~~ such threshold than other nearest airports as Keflavik. This is ~~probably~~ due to a very marked difference in the wind patterns between

the North-NorthEast and the West. ~~We can also highlight that after~~ After 48 hours since the beginning of the eruption, only ~~medium eruption class exceeds~~ Akureyri airport should exceed probabilities above 5% to reach the concentration threshold of 2 mg/m$^3$ for a Medium class eruption. No airport shows exceedance probabilities for ~~this critical threshold in ash concentration~~ such critical threshold above 25%.

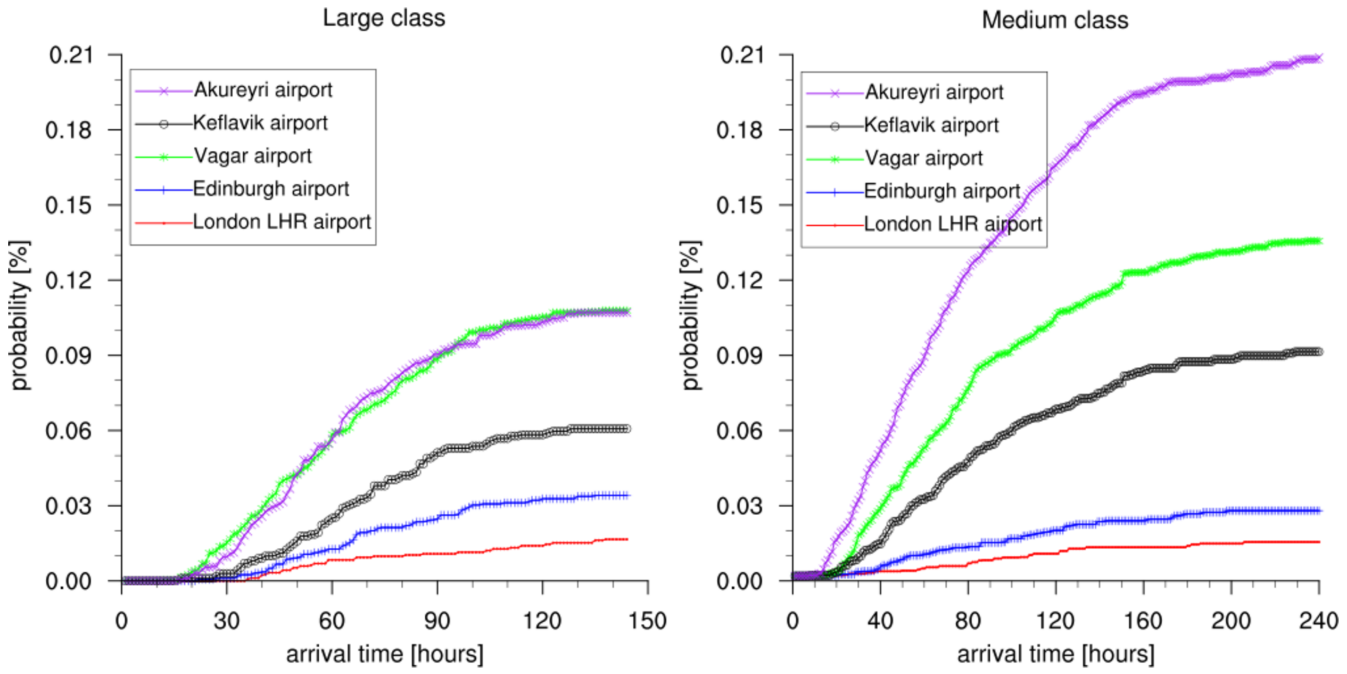


**Figure 13.** Exceedance probabilities vs arrival times required for the ash concentration (at FL050) to exceed a threshold of 2 mg/m$^3$ at different airports for Medium and Large eruptions since the beginning of the eruption.

## 5.2 Exceedance probability maps

Figures 9 and ~~?? (D1 and ?? in the appendix) show the probability of reaching or exceeding ash concentration above 0.2 mg/m$^3$ (left), 2 mg/m$^3$ (center) and 4 mg/m$^3$ (right) at 5.000 and 25.000 and anytime during the eruption up to 48 hours after its end. Concerning the size of the eruption, we first notice that the results , in terms of airborne~~ D1 in the Appendix D show substantially different results regarding ash concentration and extent for both eruption classes. Regarding concentrations, for Large class, ~~are substantially different: for large magnitude classeruptions, concentrations~~ values above 2 mg/m$^3$ (reaching even 4 mg/m$^3$, originally considered no fly zone) would affect ~~(at different flight levels)~~ part of the ~~Flight Information Region (FIR) for which Icelandic authorities are responsible,~~ Icelandic FIR with exceedance probabilities between ~~5~~ 10 and 50%~~at some time during the eruption up to 48 hours after its end~~. Instead, for ~~medium magnitude classeruptions, these~~ Medium class, such concentrations would affect only low flight levels. Above ~~25000 feet~~FL250, moderate-higher probabilities are only found

in polar routes. This is due to the fact that the height of the eruptive column for ~~medium eruptive~~ Medium magnitude class eruptions does not exceed 11 km (see ~~section~~ Section 3.1). These results are in agreement with ~~the results shown in Figures ?? and 10 , where different~~ those shown in Figure 10 (where maps, at different levels of confidence, were produced by cutting the hazard curves at ~~different percentiles~~ distinct percentiles to depict the relative uncertainties related with airborne ash cloud concentrations and extent for both eruption ~~categories at 5000 feet~~classes at FL050).

~~When analyzing~~ Concerning the extent, ~~the influence of the eruption category is also relatively important. At 5000 feet, the volcanic ash cloud with~~ at FL050, ash concentrations up to 2 mg/m$^3$ ~~, affecting maximum risk actions like takeoff or landing, could reach a large part of the UK with a probability between 2.5 and 50~~could reach almost the entire Icelandic FIR with probabilities between 10-50% for both eruption classes. It could threaten the vast majority of flights to and from northern routes. ~~However, at 25000 feet, the ash cloud would affect almost the entire FIR, even reaching part of the UK~~ Instead, at FL250, ash clouds would affect the North-East of Iceland for concentrations up to 0.2 mg/m$^3$ ~~when large size eruptions. For medium-size eruptive class, only polar routes above 25000 feet would be threatened~~only when Large size eruption occurs. Then, we can conclude that for ~~medium-size eruption~~ Medium class, only polar routes above ~~25000 feet~~ FL250 would be threatened.

Finally, ~~similar~~ in a similar way to other types of analysis such as ~~ground load of tephra~~ tephra ground load and Probabilistic Seismic Hazard Assessment, Figure 14 provides a graphical representation of relative uncertainties related with airborne ash cloud concentrations above 0.2 mg/m$^3$, 2 mg/m$^3$, and 4 mg/m$^3$ at ~~5000 feet~~ FL050 at Keflavik airport. This result, ~~that we calculate~~ computed at each point of the target domain, could be eventually used as input for risk analysis like for producing fragility curves, tolerance analysis and in general investigation of impact on infrastructure. In this view, it ~~represent~~ represents the most complete way to quantify hazard. Specifically, no dramatic differences are seen depending on the eruption size, and there is a non-negligible probability to overcome the 2 mg/m$^3$ threshold, even for low percentiles, given an eruption.

### 5.3 Persistence maps

According to Figure 7, jet engines exposed to ~~such persisting concentration conditions~~ concentration conditions of up to 4 mg/m$^3$ for more than 3 hours would require inspection. ~~Therefore, we conclude that in~~ This motivates the spatio-temporal analysis of persistent high concentration scenarios. In terms of ash cloud extent, results (Figures 11 and 12) are slightly different: ~~concerning altitude, at 5000 feet~~ at FL050 a large part of Icelandic FIR (reaching in some extent ~~UK~~Faroe island) with probabilities ~~5~~ between 10 and 50% would be affected for both eruption classes ~~, while at 25000 feet~~ up to a total of 6 hours since the eruption beginning. Instead, at FL250 (Figures D2 and D3)), such conditions would affect only high latitude air routes (above 68° N).

~~However, when analyzing the spatial pattern for long-term persistence (more~~ For high concentration scenarios longer than 12 hours~~), we find some differences depending on the eruption category. For persistence above 12 hours, at 5000 feet~~, some differences between the eruption class can be observed. At FL050, an ash cloud ~~from a large/medium eruption has 2% to~~ has probabilities lower than 10% ~~probability~~ to reach latitudes as low as ~~65~~68° N ~~/ 62~~and 66° N for Large and Medium eruption

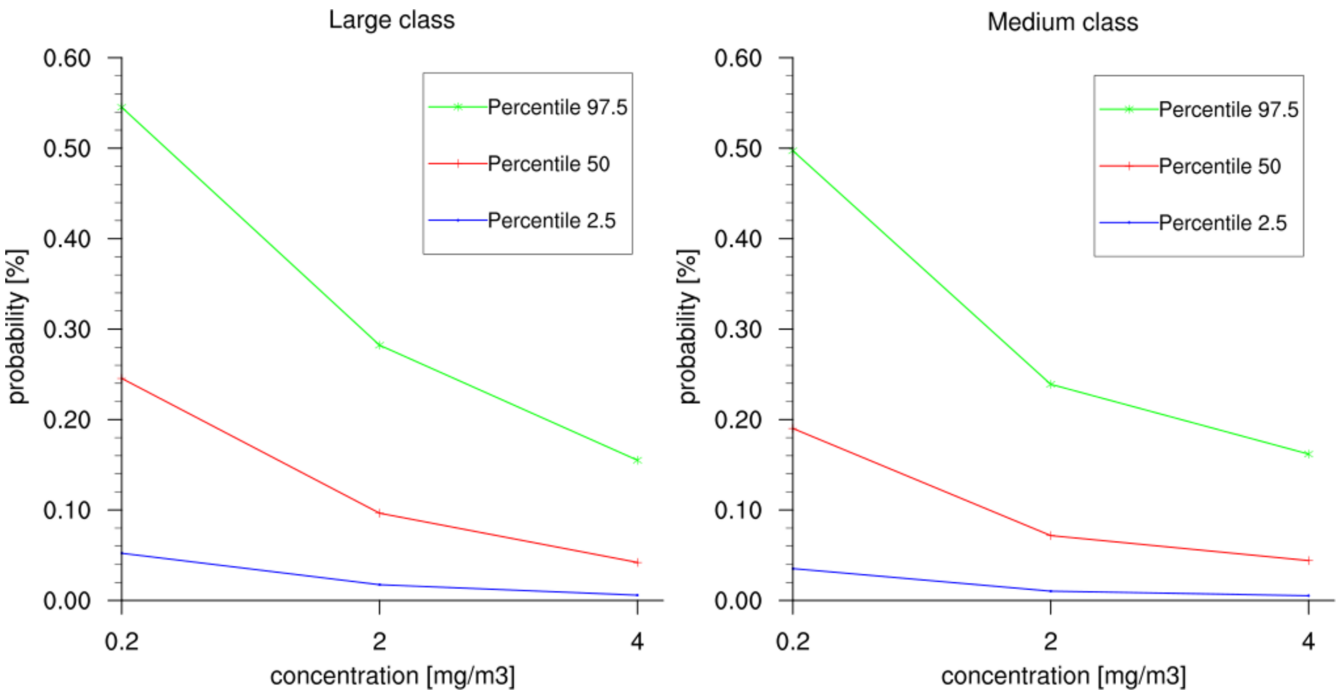


**Figure 14.** Concentration analysis: relative uncertainties related with airborne ash cloud concentrations above ~~of~~ 0.2 mg/m$^3$, 2 mg/m$^3$ and 4 mg/m$^3$ at ~~5000 feet for~~ FL050 at Keflavik airport.

respectively. Such southernmost latitude increases for longer persistence values, meaning that (obviously) only closer to the source we may get long-persisting clouds.

Finally, Figure 15 presents a persistence analysis for the airports considered in this study, showing the exceedance probability of reaching ash concentration above the critical condition for maximum risk actions like takeoff or landing ~~at different airports in Iceland and UK for at least~~ until 24 hours since the beginning of the eruption. The most affected airports are Akureyri, Vagar and Keflavik~~(London LTN and London LHR have~~ . London LHR has very low probabilities (1.5%-2%) ~~of persistence of~~ associated to 1 to 6 hours ~~only when the simulation is carried out for~~ persistence scenarios until 48 hours after the beginning of the eruption~~)~~. Concerning the level of persistence, ~~we can highlight that both eruptions categories~~ both eruption classes have similar behavior. Scenarios with persistence ~~greater~~ larger than 18 hours are highly unlikely. However, when analyzing probabilities, ~~medium eruptions reach persistence probabilities~~ Medium class reachs values twice higher than ~~large ones~~Large one. This observation can again be associated with their eruptive dynamic. The sustained injection of tephra into the atmosphere related with a series of discrete short-lived events increases the probability of prolonged ~~persistence~~ high concentration scenarios.

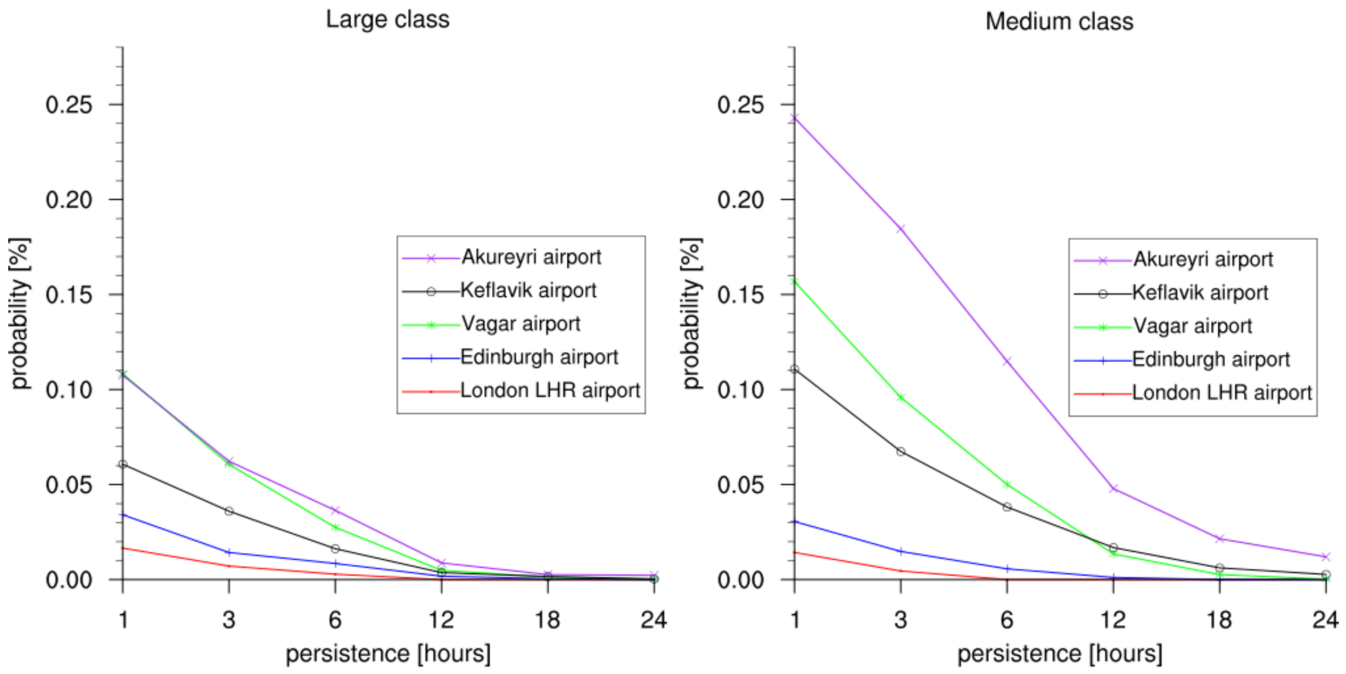


**Figure 15.** Persistence analysis for ash concentration up to 2 mg/m$^3$ at FL050. Exceedance probability of reaching or exceeding ash concentration above 2 mg/m$^3$ at ~~5000 feet~~ FL050 1 hour, 3 hours, 6 hours, 12 hours, 18 hours, 24 hours at different airports during the eruption up to 48 hours after its end.

## 6 Conclusions

~~Although limitation due to the lack of a complete geological record composed of both chronological and statistical data~~ Despite the partial geological record can be a bias for hazard assessment ~~on Jan Mayen Island~~for JM island, the spatio-temporal analysis ~~and threat assessment presented here do provide~~ presented here provides the first comprehensive analysis of potential impact on aviation safety in the ~~north~~ North Atlantic due to a future explosive activity.~~We believe that, despite the intrinsic limitations of the methodology (partially due to the scarcity of data), this work represents an important element in the long-term volcanic hazard assessment for Jan Mayen volcano of interest for key stakeholders like aviation authorities, VAACs and governments.~~

~~Among the most important conclusions, it can be highlighted that, an~~ An ash-rich eruption originating from ~~Jan Mayen~~ JM volcano has potential to affect ~~the~~ air traffic over Iceland (after 36 hours) and, to some extent, the Faroe Island, after 48 hours. Concerning airborne ash concentration and extent, for ~~large~~ Large eruptions, concentrations above 2 mg/m$^3$ (even 4 mg/m$^3$, originally considered no fly zone) would affect part of the Icelandic airspace (at different flight levels) with exceedance probabilities between ~~5~~ 10 and 50% at some time ~~during~~ from the onset of the eruption up to 48 hours after its end. For ~~medium~~ Medium eruptions, these dangerous concentrations would affect only low flight levels ~~. Above 25000 feet~~ (FL050). Above FL250 only polar routes would be affected.

When analyzing persisting concentration conditions where aircraft engines are exposed to high concentration for more than 3 hours, we conclude that at ~~5000 feet~~ FL050 a large part of icelandic FIR (reaching in some extent ~~UK~~U.K.) with probabilities 5 and 50% would be affected for both ~~medium and large eruption categories. At 25000 feet~~ Medium and Large eruption classes. At FL250 such risky conditions would affect only high latitude air routes (above 68° N).

Finally we want to highlight the robustness of our PVHA in terms of uncertainty quantification, that should be routinely considered in all this kind of studies.

*Code and data availability.* Scripts and pipeline programs will be uploaded according to the manuscript preparation guidelines

This section provides an overview about the High Performance Computing (HPC) environment used in this study and the setup process associated with the ~~Fall3d~~ FALL3D model to simulate the eruptive scenarios. ~~We will describe the~~ The most relevant settings to optimize ~~both energy and~~ the computational resources, as well as the simulation scheme followed are described.

## Appendix A: Simulation setup

~~In order to meet computational constraints, we run the experiments by months. We randomly sampled~~ To account for the meteorological statistics in the simulation results of each eruptive class (Large and Medium), 1500 wind fields ~~on the time interval~~ over the time period 1999–~~2019 from ECMWF Reanalysis database for each eruptive class (large and medium)~~2020

were randomly sampled from ECMWF ERA5 Reanalysis dataset. Then, ~~we run~~ 1500 simulations (scenarios) combining meteorological conditions and ~~volcanological parameters for each category. Since medium eruptive classes are~~ ESP for each class were run. Since Medium eruptive class is characterized by a series of discrete short-lived events, the total number of scenarios for such ~~category~~ class was 3763. The total used CPU/GPU hours was 9.6M, considering the architectures showed in Table C1 in Appendix C.

~~As can be seen in~~ Figure A1 ~~, which~~ shows the variance of the tephra concentration ~~for~~ at a given grid-point with respect to the number of scenarios simulated~~, from~~ . After 900 scenarios, the variance of the concentration begins to stabilize. This stabilization also suggests a reduction in uncertainty related to the intra-size variability of the eruptive scenarios themselves.

~~To run the scenarios , we used the~~ All the scenarios were ran using Fall3D-8.1 model (Folch et al., 2020) ~~, an open-source off-line Eulerian model for atmospheric passive transport and deposition which solves a set of advection-diffusion-sedimentation (ADS) equations on a structured terrain-following grid using a second-order Finite Differences (FD) explicit scheme. The simulation scheme was run on a (approx.) 2km-resolution~~ over a 2000 km ~~(×)~~ × 2000 km domain ~~encompassed~~ between 50°N and 73°N (on latitude) and 2°W and 24°W (on longitude) ~~. Original eruptive vents are simulated~~ with a resolution of about 2 km. Eruptive vents were placed at (70.98°N, 8.38°W) and (71.10°N ,8.13°W) respectively for Medium and Large eruptive ~~categories~~classes.

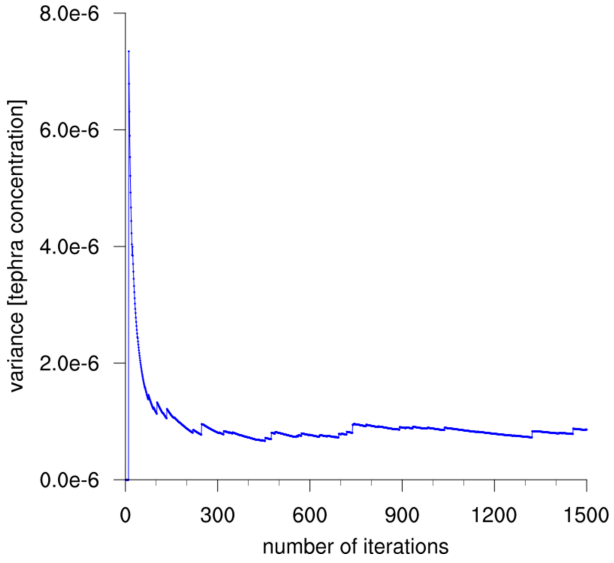


**Figure A1.** Value of the variance of tephra concentration for a given grid-point with respect to the number of scenarios simulated.

## Appendix B: Sampling and processing workflow

~~As mentioned above, in order to achieve a less biased PVHA, we should account for the uncertainty in the ESP, as well as the magnitude and intensity variability in the eruption class, in the vent position, and in the wind field. The natural approach~~

~~to do it is by simulating and appropriately combining a statistical number of representative eruptive scenarios, where each of these representative eruptive scenarios is characterized by randomly-defined eruption conditions. Such eruption conditions are composed by several eruptive parameters. Then, for~~ For each eruptive class, ~~we set the PDF for each eruptive parameter as in (Sandri et al., 2016)~~the PDFs describing each ESP were fixed following Sandri et al. (2016). It is important to note that ~~in this study we~~ this work only addressed the ~~medium and large~~ Medium and Large eruptive classes. Table B1 summarizes the PDFs and values ranges of the main ~~eruptive parameters for Jan Mayen island.~~ ESP for JM island. The sampling process can be described as:

1. Sample a value for total erupted volume (or magnitude), duration of the fallout phase, column shape ~~, total grain size distribution~~ and sphericity of tephra particles from their PDFs. The total erupted volume, expressed as DRE is computed uniformly within a range of values ($10^8$ -$10^{8.9}$ $m^3$). In a second step, we weight each total eruption volume based on the Weibull distribution function previously defined (Figure 2). ~~Doing that~~ In this way the unlikely events are properly represented.

2. Compute the mass fraction (%) associated to tephra fallout with respect to the total erupted mass according to the available estimations from field data analysis. For ~~medium~~ Medium eruptive class, the value of % is fixed to 0.8, ~~meanwhile for large~~ whereas for Large eruptive class is randomly sampled from [0.05, 0.10].

3. Compute the mass eruption rate and the column heights from total erupted volume sampled. ~~We obtain~~ The mass eruption rates ~~ranging between 6.94*10~~ranges between $3.009x10^4$ ~~-1.39*10~~-$1.5x10^6$ kg/s and ~~0.6*10$^5$-1.2*10~~$6.94x10^4$ -$1.39x10^6$ kg/s for Medium and Large eruptive sizes respectively. The source term (vertical distribution of mass in the eruption column) is given by a Suzuki distribution (Suzuki et al., 1983) with the parameter A in the range 3 to 4.5 and $\lambda = 1$.

4. Sample a time for the eruption start over a period of ~~20~~ 21 years (1999–~~2019~~2020) considering the corresponding meteorological fields for the duration of the fallout phase, and associate this randomly to a combination of the volcanological parameters. For this, ~~we download~~ ECMWF ERA5 reanalysis meteorological data have been used associated with the date and duration of the eruption.

5. ~~Run FALL3D to obtain the tephra loading at different flight levels.~~ Modify FALL3D's input file with both, meteo and newly sampled data values. ~~If the eruptive scenario assumes tephra composed of more than one type of particle, it will be necessary to create as many input files as types of particles and modify the source block independently for each of them~~

6. Run FALL3D to obtain the tephra loading at different flight levels. Ganser terminal velocity model (Ganser, 1993) and the CMAQ model parameterization for horizontal diffusion (Folch et al., 2009) were used as part of model physics configuration.

**Table B1.** PDFs and values ranges of the main eruptive parameters for ~~Jan Mayen~~ JM island. Bounds on Mass Eruption Rate values are a consequence of the sampling procedure for total erupted volume (Figure 3) and duration of the fallout phase described in the text. For the total grain size distribution, references were chosen from Eggoya 1732 and Grimsvönt 2004 eruptions for ~~medium and large categories respectively. Considering an average densities of $13*10^3$ and $12*10^3$ kg/m$^3$ for~~ Medium and Large ~~eruptions~~ classes respectively~~, erupted~~. Erupted volumes are between 0.1–0.5, and >0.5 km$^3$ for Medium, and Large ~~categories~~ classes ranges.

| Parameter | Eruption Class | PDF type and ranges |
|---|---|---|
| Total erupted volume (Kg[a]) | Medium | Weibull on $[10^8;10^{8.7}]$ |
| | Large | Weibull on $[10^{8.7};10^{8.9}]$ |
| Duration of fallout (hours) | Medium | Uniform on [96;960] composed by pulses |
| | Large | Uniform on [24;120] |
| Mass eruption rate (kg/s) | Medium | ~~Uniform on~~ $[3.009*10^4;1.5*10^6]$ |
| | Large | $[6.94$~~$*10$~~x$10^4;1.39$~~$*10$~~x$10^6]$ |
| Total Grain Distribution modes (Φ- units) | Medium | Eggoya 1732 Surtseyan eruption reference |
| | Large | Grimsvötn 2004 eruption reference |
| Density of tephra particles (kg/m$^3$) | Medium | 1300 |
| | Large | 1200 |
| Tephra mass fraction (%) | Medium | 80 |
| | Large | Uniform on [5;10] |
| Density of particles aggregates (kg/m$^3$) | both types | Aggregate 1: 250 |
| | | Aggregate 2: 350 |
| Diameter of particles aggregates (Φ- units) | both types | Aggregate 1: 100 |
| | | Aggregate 2: 250 |

7. ~~Once the eruptive scenario has been built, it is run in the framework of High performance Computing (HPC). To do that, we use TGCC Joliot Curie, the most powerful French supercomputer dedicated to French and European research.~~

8. ~~The results obtained are computed using PVHA-WF software~~The outputs obtained from FALL3d are computed. As a result, ~~we obtain~~ hazard and probabilistic maps describing the airborne ash concentration and time-persistence at different flight levels on a large-scale and high-resolution domain are obtained.

Typical tephra particle densities and total grain size distributions were chosen consistent with previous values reported for Eggoya (1790) and ~~Grimsvotn~~ Grimsvötn (2004) eruptions for Medium and Large ~~categories respectively. Regarding the type and spatiotemporal distribution of aggregates (ash particles with diameters <63 $\mu$m settle from eruption clouds and adhere to each other as a result of electrostatic attraction, moist adhesion between particles and hydrometeor formation)~~ classes respectively. The type of aggregates were also chosen consistent with previous values reported for similar ~~surtseyan~~ Surtseyan and phreatomagmatic eruptions.

## Appendix C: Computational resource

Experiments were run on Joliot-Curie, at ~~CEA~~Très Grand Centre de calcul du CEA (The French Alternative Energies and Atomic Energy Commission (CEA) /~~TGCC (a relevant HPC environment dedicated to French and European research). We had two partitions assigned, Irene-rome and Irene-skylake (see Table C1 for specifications)with a total of 63M core hours~~TGCC).

~~When working in HPC environments, it is mandatory to find the optimal configuration of both the number of cores and nodes used in order to optimize the energy consumption and computing time.~~ Considering that FALL3D-8.1 uses MPI for 3D domain decomposition with freedom for the user to choose the number of processors along each spatial direction, to identify the optimal running configuration on Irene-rome and Irene-skylake, ~~we run~~ a few benchmark cases (with grid size similar to that of the real benchmark ones, 50M grid points and 12 particle bins) were ran changing the configuration of nodes and cores used. Results are shown in Figure C1.

**Table C1.** Joliot- Curie supercomputer. Characteristics corresponding with the two partitions available on this study.

| Machine | Institution | Hardware |
|---|---|---|
| Irene-Rome | CEA/TGCC | 2292 AMD Rome 2.6GHz bi-processor compute nodes with 128 cores per node (64x2).This totals 293376 compute cores and 11.75 PFlop/s peak power. |
| Irene-Skylake | CEA/TGCC | 1656 Intel-skylake 2.7GHz bi-processor compute nodes with 48 cores per node (24x2).This totals 79488 cores with 180GBy/node. |

As observed, for this particular grid size, parallel efficiencies are substantially better at Irene-rome, with >90% up to 2048 processors (16 nodes). At the Irene-skylake partition, parallel efficiencies already drop to 70% with only 1036 processors (32 nodes). Scalability breaking at a larger number of processors occurs because the number of grid points per sub-domain

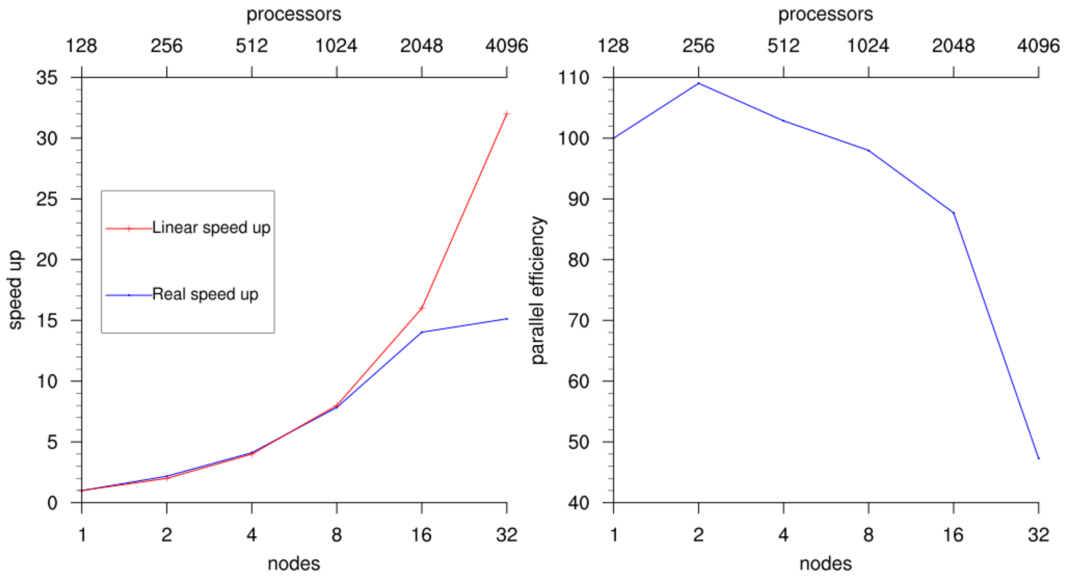


Irene Rome

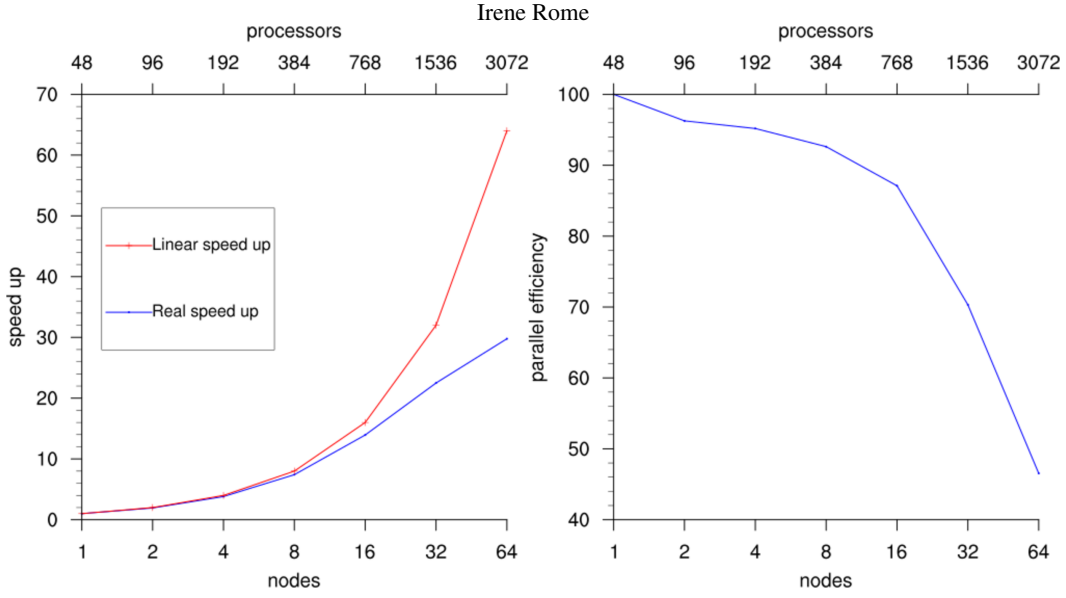


Irene Skylake

**Figure C1.** Strong scalability analysis (time to solution). Top: speed-up and parallel efficiency analysis at Irene-rome (128 AMD processors per node). Bottom: same for Irene-skylake (48 skylake processors per node).

becomes less than the specific range in which communications start to overtake computations (a larger grid size would be needed to sustain speed-up ratios close to optimal above 2048 processors). Then, considering the resolution of our domain (0.025º), and the total grid points 35M (~~1040*920*35~~1040x920x35x14), we fixed the number of nodes to 16 and the number of cores to 768. This configuration allows decomposing the grid points into ~~32*24*1~~ 32x24x1 (X, Y, Z) subdomains of more than 30 points per spatial dimension. As a result, we increased the speed-up 16 times and the parallel efficiency was fixed to 90%.

## Appendix D: Complementary maps

### D1 Exceedance probability maps at ~~25000 feet~~FL250

~~Figures D1 and ?? show~~ Figure D1 shows the exceedance probability maps computed at ~~25000 feet~~FL250.

~~Exceedance probability (Medium): probability of reaching or exceeding ash concentration above 0.2 mg/m$^3$ (left), 2 mg/m$^3$ (center) and 4 mg/m$^3$ (right) at 25000 at some time during the eruption up to 48 hours after its end.~~

### D2 Persistence maps at ~~25000 feet~~FL250

Figures D2 and D3 show the exceedance probability maps computed at ~~25000 feet~~FL250.

*Author contributions.* Sara Barsotti, Laura Sandri, Arnau Folch, Giovanni Macedonio, and Antonio Costa contributed to the conception and design of study, analysis and/or interpretation of data and drafting the manuscript. Manuel Titos, Beatriz Martinez Montesinos and Leonardo Mingari contributed to coding the scripts and software, analysis and/or interpretation of data and drafting the manuscript.

*Competing interests.* The authors declare that author Giovanni Macedonio is a member of the editorial board of the journal.

*Acknowledgements.* The research leading to these results has received funding from the European Union's Horizon 2020 research and innovation programme under the ChEESE project, grant agreement N° 823844.We ~~acknowledge PRACE for awarding us access to Joliot-Curie at GENCI@CEA, France. We would like to thank our colleagues Paolo Perfetti, Roberto Tonini and Jacopo Selva for the prototype tool BET OV, which was used as starting point for building the workflow used in this study~~thank the multi-year PRACE Project Access "Volcanic Ash Hazard and Forecast" (ID 2019215114).

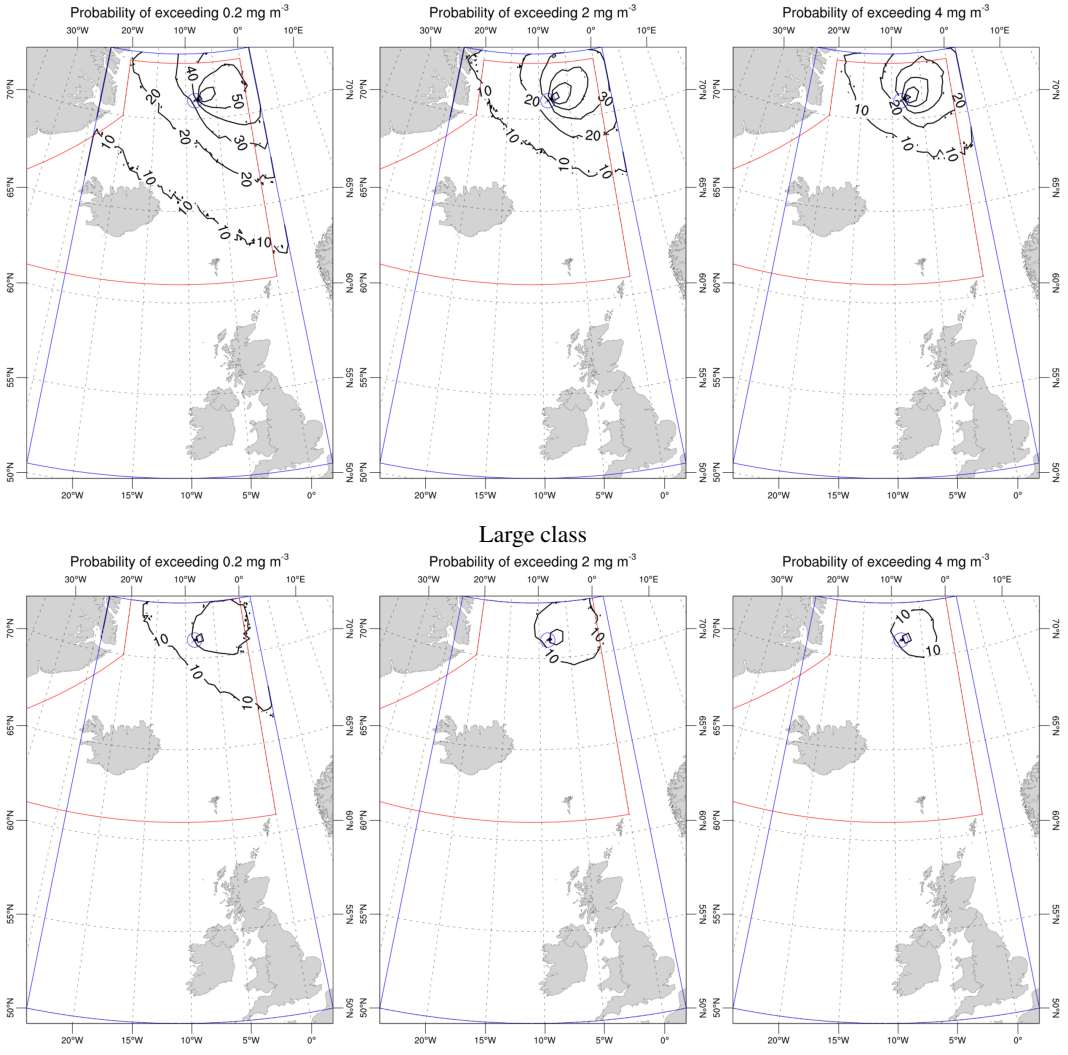


**Figure D1.** Exceedance probability ~~(Large)~~maps at FL250: the isolines show the probability of reaching ~~or exceeding~~ ash concentration above 0.2 mg/m$^3$ (left), 2 mg/m$^3$ (center) and 4 mg/m$^3$ (right) at ~~25000 feet~~ FL250 at some time ~~during~~ from the onset of the eruption up to 48 hours after its end.

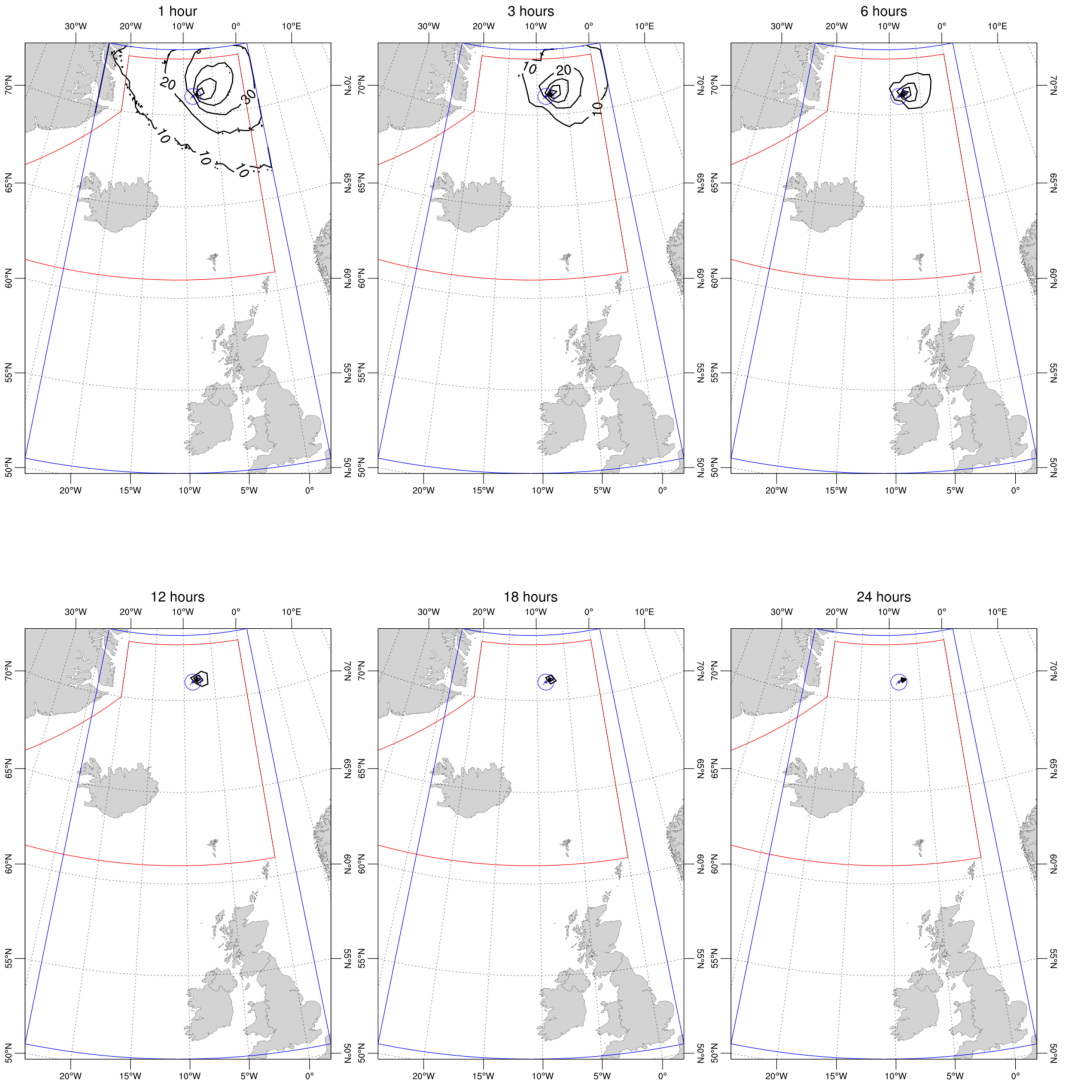


**Figure D2.** ~~Exceedance probability~~ Persistence maps at FL250 (Large class): the isolines show probability of reaching or exceeding ash concentration above 2 mg/m$^3$ at ~~25000 feet~~ FL250 1 hour, 3 hours, 6 hours, 12 hours, 18 hours, 24 hours during the eruption up to 48 hours after its end.

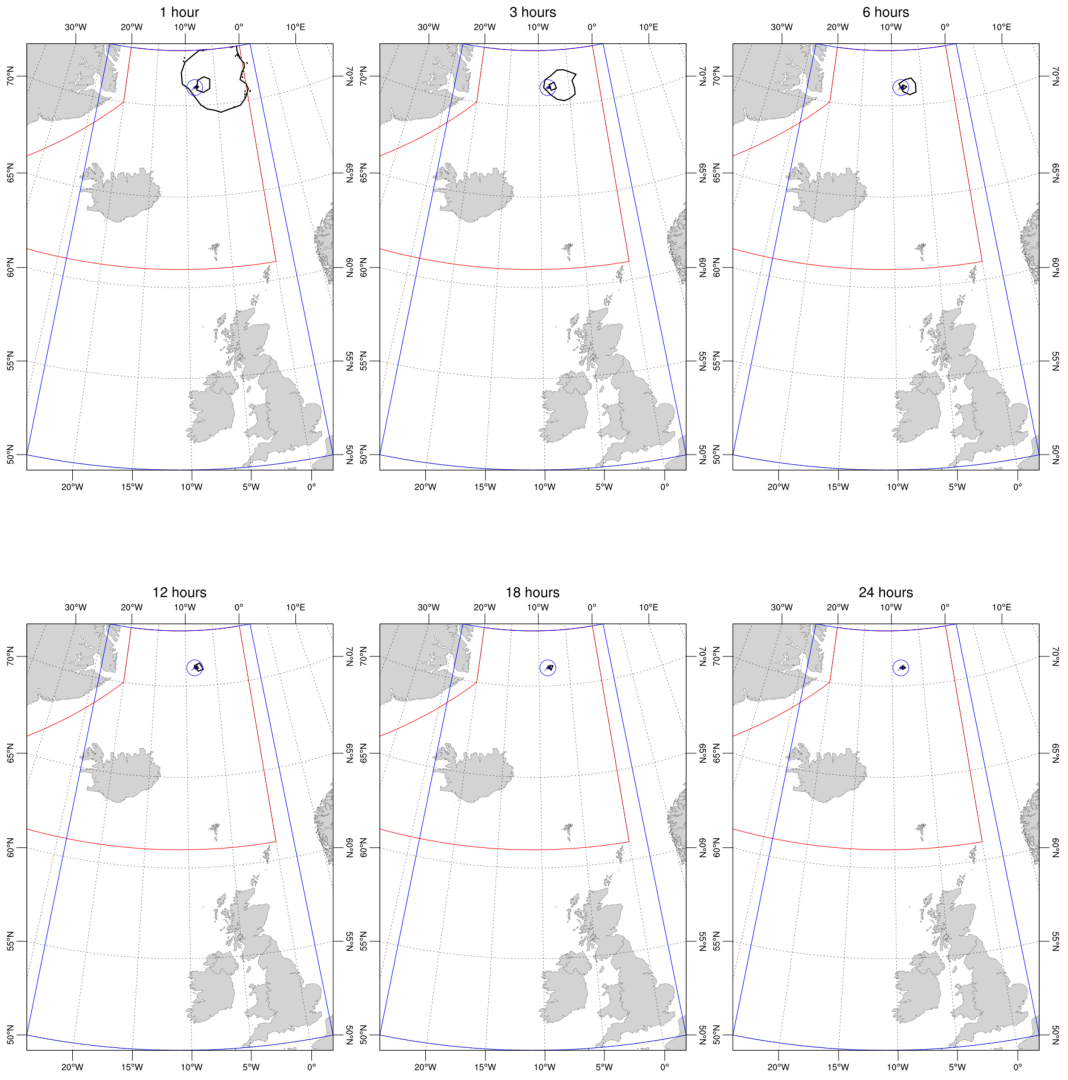


**Figure D3.** ~~Exceedance probability~~ Persistence maps at FL250 (Medium class): the isolines show probability of reaching or exceeding ash concentration above 2 mg/m$^3$ at ~~25000 feet~~ FL250 1 hour, 3 hours, 6 hours, 12 hours, 18 hours, 24 hours during the eruption up to 48 hours after its end.

## References


Abbott, P. M. and Davies, S. M.: Volcanism and the Greenland ice-cores: the tephra record, Earth-Science Reviews, 115, 173–191, 2012.

Akaike, H.: Information theory and an extension of the maximum likelihood principle, in: Selected papers of hirotugu akaike, pp. 199–213, Springer, 1998.

Amante, C. and Eakins, B. W.: ETOPO1 arc-minute global relief model: procedures, data sources and analysis, 2009.

Barsotti, S., Di Rienzo, D. I., Thordarson, T., Björnsson, B. B., and Karlsdóttir, S.: Assessing impact to infrastructures due to tephra fallout from Öræfajökull volcano (Iceland) by using a scenario-based approach and a numerical model, Frontiers in Earth Science, 6, 196, 2018.

Blischke, A., Gaina, C., Hopper, J., Péron-Pinvidic, G., Brandsdóttir, B., Guarnieri, P., Erlendsson, Ö., and Gunnarsson, K.: The Jan Mayen microcontinent: an update of its architecture, structural development and role during the transition from the Ægir Ridge to the mid-oceanic Kolbeinsey Ridge, Geological Society, London, Special Publications, 447, 299–337, 2017.

Bonadonna, C., Connor, C. B., Houghton, B., Connor, L., Byrne, M., Laing, A., and Hincks, T.: Probabilistic modeling of tephra dispersal: Hazard assessment of a multiphase rhyolitic eruption at Tarawera, New Zealand, Journal of Geophysical Research: Solid Earth, 110, 2005.

Bozdogan, H.: Model selection and Akaike's information criterion (AIC): The general theory and its analytical extensions, Psychometrika, 52, 345–370, 1987.

Brendryen, J., Haflidason, H., and Sejrup, H. P.: Norwegian Sea tephrostratigraphy of marine isotope stages 4 and 5: prospects and problems for tephrochronology in the North Atlantic region, Quaternary Science Reviews, 29, 847–864, 2010.

Budd, L., Griggs, S., Howarth, D., and Ison, S.: A fiasco of volcanic proportions? Eyjafjallajökull and the closure of European airspace, Mobilities, 6, 31–40, 2011.

Budnitz, R., Apostolakis, G., and Boore, D. M.: Recommendations for probabilistic seismic hazard analysis: guidance on uncertainty and use of experts, Tech. rep., Nuclear Regulatory Commission, Washington, DC (United States). Div. of Engineering Technology; Lawrence Livermore National Lab., CA (United States); Electric Power Research Inst., Palo Alto, CA (United States); USDOE, Washington, DC (United States), 1997, 1997.

Clarkson, R. J., Majewicz, E. J., and Mack, P.: A re-evaluation of the 2010 quantitative understanding of the effects volcanic ash has on gas turbine engines, Proceedings of the Institution of Mechanical Engineers, Part G: Journal of Aerospace Engineering, 230, 2274–2291, 2016.

Elefante, L., Jalayer, F., Iervolino, I., and Manfredi, G.: Disaggregation-based response weighting scheme for seismic risk assessment of structures, Soil Dynamics and Earthquake Engineering, 30, 1513–1527, 2010.

Elissondo, M., Baumann, V., Bonadonna, C., Pistolesi, M., Cioni, R., Bertagnini, A., Biass, S., Herrero, J.-C., and Gonzalez, R.: Chronology and impact of the 2011 Cordón Caulle eruption, Chile, Natural Hazards and Earth System Sciences, 16, 675–704, 2016.

Ellis, M., Bojdo, N., Filippone, A., and Clarkson, R.: Monte Carlo Predictions of Aero-Engine Performance Degradation Due to Particle Ingestion, Aerospace, 8, 146, 2021.

Folch, A. and Sulpizio, R.: Evaluating long-range volcanic ash hazard using supercomputing facilities: application to Somma-Vesuvius (Italy), and consequences for civil aviation over the Central Mediterranean Area, Bulletin of Volcanology, 72, 1039–1059, 2010.

Folch, A., Costa, A., and Macedonio, G.: FALL3D: A computational model for transport and deposition of volcanic ash, Computers & Geosciences, 35, 1334–1342, 2009.

Folch, A., Mingari, L., Gutierrez, N., Hanzich, M., Macedonio, G., and Costa, A.: FALL3D-8.0: a computational model for atmospheric transport and deposition of particles, aerosols and radionuclides–Part 1: Model physics and numerics, Geoscientific Model Development, 13, 1431–1458, 2020.

Ganser, G. H.: A rational approach to drag prediction of spherical and nonspherical particles, Powder technology, 77, 143–152, 1993.

Gernigon, L., Blischke, A., Nasuti, A., and Sand, M.: Conjugate volcanic rifted margins, seafloor spreading, and microcontinent: Insights from new high-resolution aeromagnetic surveys in the Norway Basin, Tectonics, 34, 907–933, 2015.

Gjerløw, E., Höskuldsson, A., and Pedersen, R.-B.: The 1732 Surtseyan eruption of Eggøya, Jan Mayen, North Atlantic: deposits, distribution, chemistry and chronology, Bulletin of Volcanology, 77, 1–21, 2015.

Gjerløw, E., Haflidason, H., and Pedersen, R.: Holocene explosive volcanism of the Jan Mayen (island) volcanic province, North-Atlantic, Journal of Volcanology and Geothermal Research, 321, 31–43, 2016.

Harvey, N. and Dacre, H.: Spatial evaluation of volcanic ash forecasts using satellite observations, Atmospheric Chemistry and Physics, 16, 861–872, 2016.

Harvey, N. J., Huntley, N., Dacre, H. F., Goldstein, M., Thomson, D., and Webster, H.: Multi-level emulation of a volcanic ash transport and dispersion model to quantify sensitivity to uncertain parameters, Natural hazards and earth system sciences, 18, 41–63, 2018.

Hill, L., Sparks, R., and Rougier, J.: Risk assessment and uncertainty in natural hazards, Risk and uncertainty assessment for natural hazards, edited by: Rougier, JC, Sparks, RS J., and Hill, LJ, pp. 1–18, 2013.

Hunt, J. B.: Tephrostratigraphical evidence for the timing of Pleistocene explosive volcanism at Jan Mayen, Journal of Quaternary Science, 19, 121–136, 2004.

ICAO: VOLCANIC ASH CONTINGENCY PLAN-EUROPEAN AND NORTH ATLANTIC REGIONS, https://www.icao.int/EURNAT/EUR%20and%20NAT%20Documents/EUR+NAT%20VACP%20v2.0.1-Corrigendum.pdf, 2021.

Imsland, P.: The geology of the volcanic island Jan Mayen, Arctic Ocean, Nordic Volcanological Institute, 1978.

Isavia: :annual report, https://www.isavia.is/annualreport2019/economy/flight-statistics, 2019.

Jakobsson, M., Mayer, L., Coakley, B., Dowdeswell, J. A., Forbes, S., Fridman, B., Hodnesdal, H., Noormets, R., Pedersen, R., Rebesco, M., et al.: The international bathymetric chart of the Arctic Ocean (IBCAO) version 3.0, Geophysical Research Letters, 39, 2012.

Kandilarov, A., Mjelde, R., Pedersen, R.-B., Hellevang, B., Papenberg, C., Petersen, C.-J., Planert, L., and Flueh, E.: The northern boundary of the Jan Mayen microcontinent, North Atlantic determined from ocean bottom seismic, multichannel seismic, and gravity data, Marine Geophysical Research, 33, 55–76, 2012.

Karlsdóttir, S., Gylfason, Á. G., Höskuldsson, Á., Brandsdóttir, B., Ilyinskaya, E., Gudmundsson, M. T., Högnadóttir, Þ., and Þorkelsson, B.: The 2010 Eyjafjallajökull eruption, Iceland, Report to ICAO, 209p, 2012.

Kristiansen, N., Stohl, A., Prata, A., Bukowiecki, N., Dacre, H., Eckhardt, S., Henne, S., Hort, M., Johnson, B., Marenco, F., et al.: Performance assessment of a volcanic ash transport model mini-ensemble used for inverse modeling of the 2010 Eyjafjallajökull eruption, Journal of Geophysical Research: Atmospheres, 117, 2012.

Lacasse, C. and Garbe-Schönberg, C.-D.: Explosive silicic volcanism in Iceland and the Jan Mayen area during the last 6 Ma: sources and timing of major eruptions, Journal of Volcanology and Geothermal Research, 107, 113–147, 2001.

Larsen, E., Lysså, A., Höskuldsson, Á., Davidsen, J. G., Nadeau, M. J., Power, M., Tassis, G., and Wastegård, S.: A dated volcano-tectonic deformation event in Jan Mayen causing landlocking of Arctic charr, Journal of Quaternary Science, 36, 180–190, 2021.

Larsen, G. and Guðmundsson, M. T.: Catalogue of Icelandic Volcanoes, http://icelandicvolcanoes.is/?volcano=BEE, 2016.

Larsen, G., Gudmundsson, M., and Oladottir, B.: Catalogue of Icelandic Volcanoesn, Report, IMO, UI and CPD-NCIP, 2017.

Macedonio, G., Costa, A., and Folch, A.: Ash fallout scenarios at Vesuvius: numerical simulations and implications for hazard assessment, Journal of Volcanology and Geothermal Research, 178, 366–377, 2008.

Mastin, L. G., Guffanti, M., Servranckx, R., Webley, P., Barsotti, S., Dean, K., Durant, A., Ewert, J. W., Neri, A., Rose, W. I., et al.: A multidisciplinary effort to assign realistic source parameters to models of volcanic ash-cloud transport and dispersion during eruptions, Journal of Volcanology and Geothermal Research, 186, 10–21, 2009.

Mazzocchi, M., Hansstein, F., and Ragona, M.: The 2010 volcanic ash cloud and its financial impact on the European airline industry, in: CESifo Forum, vol. 11, pp. 92–100, München: ifo Institut für Wirtschaftsforschung an der Universität München, 2010.

NavCanada: Polar routes – past, present and future, https://www.navcanada.ca/en/news/blog/polar-routes--past-present-and-future.aspx, 2017.

Newhall, C. G. and Self, S.: The volcanic explosivity index (VEI) an estimate of explosive magnitude for historical volcanism, Journal of Geophysical Research: Oceans, 87, 1231–1238, 1982.

Oxford-economics: The economics impacts of air travel restrictions due to volcanic ash., https://www.oxfordeconomics.com/my-oxford/projects/129051, 2010.

Peron-Pinvidic, G., Gernigon, L., Gaina, C., and Ball, P.: Insights from the Jan Mayen system in the Norwegian–Greenland sea—I. Mapping of a microcontinent, Geophysical Journal International, 191, 385–412, 2012.

Prata, A. T., Dacre, H. F., Irvine, E. A., Mathieu, E., Shine, K. P., and Clarkson, R. J.: Calculating and communicating ensemble-based volcanic ash dosage and concentration risk for aviation, Meteorological Applications, 26, 253–266, 2019.

Pyle, D. M.: Sizes of volcanic eruptions, in: The encyclopedia of volcanoes, pp. 257–264, Elsevier, 2015.

Rory, C.: Volcanic Ash Impacts on Jet Engines and Developments Since 2010, Tech. rep., Engine Environmental Protection Rolls-Royce (Aero Engines), 2010.

Sandri, L., Costa, A., Selva, J., Tonini, R., Macedonio, G., Folch, A., and Sulpizio, R.: Beyond eruptive scenarios: assessing tephra fallout hazard from Neapolitan volcanoes, Scientific reports, 6, 1–13, 2016.

Siggerud, T.: The volcanic eruption on Jan Mayen 1970, Norsk Polarinstitutt Arbok, 1970, 5–18, 1972.

Stewart-Green, C.: ANS Planning: NAV CANADA, https://www.icao.int/NACC/Documents/Meetings/2016/ASBU/ASBUP12.pdf, 2016.

Sulpizio, R., Folch, A., Costa, A., Scaini, C., and Dellino, P.: Hazard assessment of far-range volcanic ash dispersal from a violent Strombolian eruption at Somma-Vesuvius volcano, Naples, Italy: implications on civil aviation, Bulletin of Volcanology, 74, 2205–2218, 2012.

Suzuki, T. et al.: A theoretical model for dispersion of tephra, Arc volcanism: physics and tectonics, 95, 113, 1983.

Tesche, M., Glantz, P., Johansson, C., Norman, M., Hiebsch, A., Ansmann, A., Althausen, D., Engelmann, R., and Seifert, P.: Volcanic ash over Scandinavia originating from the Grímsvötn eruptions in May 2011, Journal of Geophysical Research: Atmospheres, 117, 2012.

Voelker, A. H. and Haflidason, H.: Refining the Icelandic tephrachronology of the last glacial period–the deep-sea core PS2644 record from the southern Greenland Sea, Global and Planetary Change, 131, 35–62, 2015.

Ward, P. L.: What really causes global warming?: greenhouse gases or ozone depletion?, Morgan James Publishing, 2015.

Woodhouse, M. J., Hogg, A. J., Phillips, J. C., and Rougier, J. C.: Uncertainty analysis of a model of wind-blown volcanic plumes, Bulletin of volcanology, 77, 1–28, 2015.